A&A 537, A57 (2012)
DOI: 10.1051/0004-6361/201014160

Astronomy & Astrophysics

The slowly declining type Ia supernova 2008fv and the near-infrared second maximum⋆

I. Biscardi[1,2], E. Brocato[1], A. Arkharov[3], E. Di Carlo[1], G. Di Rico[1], M. Dolci[1], N. V. Efimova[3], A. Pietrinferni[1], and G. Valentini[1]

[1] INAF-Osservatorio Astronomico di Teramo, via M. Maggini s.n.c., 64100 Teramo, Italy
e-mail: biscardi@oa-teramo.inaf.it
[2] Dipartimento di Fisica – Università di Roma Tor Vergata, via della Ricerca Scientifica 1, 00133 Rome, Italy
[3] Central Astronomical Observatory at Pulkovo, Pulkovskoe Shosse 65, 196140 St. Petersburg, Russia

Received 25 January 2010 / Accepted 12 October 2011

ABSTRACT

Aims. We present optical and near-infrared (NIR) photometry of supernova (SN) 2008fv and a brief investigation of SN type Ia to search for possible correlations between the properties of NIR light curves and the optical decline rate.
Methods. We analyse our BVRI and JHK observations to derive light curves (LCs), colour curves, and the bolometric behaviour of SN 2008fv. Data range from about five days before to two months after maximum. We also collect a database of the main characteristics of NIR LCs of SNe Ia available in literature.
Results. We find close similarities between the observed LCs of the SN event studied here and SN 2000E. SN 2008fv is a slow-declining SNe Ia with a post-maximum decline of $\Delta m_{15,B} = 0.96 \pm 0.08$ mag and a B-band maximum luminosity of $M_{B,0} = -19.40 \pm 0.1$ mag, close to the value of normal SNe Ia. The optical and NIR data allow us to constrain the host galaxy reddening of NGC 3147, $E(B-V) = 0.22 \pm 0.05$ mag and its distance $\mu = 33.2 \pm 0.1$ mag. Furthermore, we derive a synthesized ^{56}Ni mass of about 0.7 $M_{\odot}$, by using the well-known relation between the maximum luminosity of the *uvoir* bolometric light curve and the initial content of ^{56}Ni. We investigate the correlation between the NIR characteristics of LCs and optical properties by collecting data of a sample of 40 SNe. We derive quantitative relationships involving the epoch of the secondary maximum in the JHK bands and the decline rate $\Delta m_{15}(B)$. Further, we find no correlations between Δm_{15} measured in the JHK bands and the optical $\Delta m_{15}(B)$. In contrast, quite evident correlations with the $\Delta m_{15}(B)$ and $\Delta m_{40}(J)/\Delta m_{15}(H)$.

Key words. galaxies: individual: NGC 3147 – supernovae: general – supernovae: individual: SN 2008fv – stars: distances

1. Introduction

One of the reasons why type Ia supernovae (SNe Ia) are considered as powerful distance indicators is that their luminosities at maximum can be calibrated via several empirical relationships. It is undeniable that large efforts have been made to improve the precision and accuracy of these relationships, but the main challenge of extending the method to wavelengths less affected by interstellar absorption remains ongoing (e.g., for a review Hicken et al. 2009). Similarly, our understanding of the physics that causes the observed variation with time of the light emitted by SNe Ia remains incomplete. It is therefore essential to continue in our multi-wavelength observations of SN Ia LCs to improve our knowledge of SN Ia events (Folatelli et al. 2010).

A number of different methods have been developed to measure calibrated distances from SN Ia multi-colour light curves in the optical bands. The first of these was introduced by Phillips (1993) and Phillips et al. (1999), who noted that the parameter $\Delta m_{15}(B)$, i.e. the magnitude decline in the B-band LC from its peak to 15 days after peak, is well-correlated with SN Ia intrinsic luminosity. Improved relations have been provided by several authors in the past fifteen years, which have also involved a "second" parameter (e.g., the colour $(B-V)$, Tripp 1998; Tripp & Branch 1999; Reindl et al. 2005), which provides a tight calibration of the luminosity. Other methods have been developed, such as the multicolour light-curve shape (MLCS) method of Riess et al. (1996), the stretch correction methods of Perlmutter et al. (1997), the SALT technique by Guy et al. (2005), and the CMAGIC technique proposed by Wang et al. (2003), who derived the absolute magnitude as a function of colour.

Each of the empirical relations cited above requires an extremely good calibration, to use the SNe Ia as reliable absolute distance indicator. In this respect, the main problems are the accuracy of independent distance determinations of nearby events and reddening effects. Thus, owing to systematic effects, the intrinsic dispersion in the peak brightness remains smaller than ∼0.2 mag depending on the specific filter. As a consequence, the distance measurement uncertainty is at most 10% (Wang et al. 2006). Being less affected by interstellar absorption, the near-infrared observations show that SNe Ia are generally quite homogeneous in this wavelength range at the level of ∼0.15 mag (Meikle 2000; Krisciunas et al. 2004a; Wood-Vasey et al. 2008; Folatelli et al. 2010), leading to distance estimates with an accuracy higher than 7%.We note that the scatter in the Hubble diagram indicated that very precise relative distances can be obtained by means of SNe Ia. Folatelli et al. (2010) suggest that the resulting scatter in the Hubble diagram is limited by the peculiar velocities of the host galaxy. This implies that the actual precision of SNe Ia distances is 3–4%.

However, the morphology of the NIR LCs of SNe Ia differs from those at optical wavelengths. The IJHK-band LCs

⋆ Tables 6, 7 and 15 are available in electronic form at http://www.aanda.org

are indeed characterized by a secondary maximum, occurring roughly 20 to 30 days after the initial one (e.g., Elias et al. 1981, 1985; Phillips et al. 2003). At the same epoch, a corresponding "shoulder" is often seen in the R and V-band LC, while the bolometric LC shows an inflection (Contardo et al. 2000). In the I-band, the properties of the secondary maximum are found to correlate with the $\Delta m_{15}(B)$ of the supernova, and to be both more prominent and to occurr later in the broader/brighter SNe Ia (Hamuy et al. 1996a; Nobili et al. 2005). Very sub-luminous objects may completely lack a secondary maximum. Similar trends appear in the J, H, and K-band LC (Krisciunas et al. 2004b), although interesting exceptions have been sought out (e.g., SN 2000cx Candia et al. 2003). Despite the theoretical insights (e.g., Hoflich et al. 1995; Wheeler et al. 1998; Pinto & Eastman 2000a,b; Kasen 2006), the origin of the NIR secondary maximum and its dependence on the SN ejecta properties remain unclear. These NIR LCs therefore provide promising means of investigating a possible empirical secondary parameter, which may explain the deviations from the standard width-luminosity relation (Kasen 2006), and thus help us to understand the intrinsic differences among SNe Ia. For this reason, the contemporary availability of NIR and optical observations plays a fundamental role in observational programs.

Here, we present the optical (BVRI) and near-infrared (JHK) photometric observations of SN 2008fv, ranging from 4 d before maximum light to 50 d after maximum. In Sect. 2 we present both the observations and data reduction of SN 2008fv as well as the characterization of the photometric systems used to measure optical and NIR magnitudes and we derive the K-correction of the SN. In Sect. 3 the optical and NIR LCs and colour curves of SN 2008fv are displayed and analysed and, we describe our main results for both SN 2008fv and the host galaxy (reddening of host galaxy, distance measurements, estimate of Ni mass). On the basis of available NIR observations of SNe Ia together with our new data on SN 2008fv, we present, in the Sect. 4, the discussion about the empirical relations between relevant features of the NIR LCs and the optical decline rate $\Delta m_{15}(B)$. A brief summary of our results is reported in the conclusion (Sect. 5).

2. Observations

2.1. SN 2008fv and host galaxy NGC 3147

SN 2008fv (α(2000.0) = $10^h16^m57.3^s$, δ(2000.0) = +73°24′ 36″) was discovered on 27 September 2008 by Koichi Itagaki at 16″ east and 34″ north of the center of the barred spiral galaxy NGC 3147, hosting a Seyfert 2 active galactic nucleus (see Table 1 for the main parameters of the galaxy). It was identified as a normal type Ia SN by Challis (2008) based on a spectral observation performed with the MMT (+ Blue Channel Spectrograph) at Mt. Hopkins. Unusually, NGC 3147 has hosted four SNe explosions in the past ∼40 years: SN 1972H (SN Ia with Δm_{15} = 1.05, Patat et al. 1997), SN 1997bq (SN Ia with Δm_{15} = 1.01, Jha et al. 2006), SN 2006gi (SN Ib, Duszanowicz 2006), and SN 2008fv, all in different regions of the galaxy. To date, about 50 galaxies have been the site of more than one SN detection: the record is for NGC 6946, where nine SNe have been detected, all type II SNe. NGC 5236 has hosted six SNe and there are three galaxies with five SNe (NGC 4303, NGC 4321, and NGC 2276). Furthermore, there are nine galaxies for which four SNe have been detected, one of which is NGC 3147. Thus, we make a short numerical exercise to investigate whether the occurrence of four recent supernovae in this galaxy should be considered as quite normal. As a starting point, we assume a SNe rate (SNR) of 0.17 for SNe Ia, 0.12 for SNe Ib/c, and 0.74 for SNe II, which are all given per century and per 10^{10} $M_\odot$ (SNuM), and refer to galaxies of morphological type Sbc/d (Mannucci et al. 2005). By the same authors, we also assume that the mass of the galaxy, i.e. a (stellar) mass of 2.5×10^{10} $M_\odot$, corresponds to the peak value of the mass distribution for Sbc galaxies. Thus, it follows that only ∼0.2 SNe Ia, ∼0.1 SNe Ib/c, and ∼0.7 SN II explosions are expected every 40 years in NGC 3147. These values are lower than those observed for both SNe Ia and SNe Ib/c, while the number of expected SNe II is close to those inferred from the observations, owing to the lack of SN II in NGC 3147. After repeating the same numerical test, and assuming the mass equals to the highest galaxy mass value of the same distribution, i.e. 1×10^{11} $M_\odot$, our results are not significantly modified. On the basis of these numerical estimates it seems that NGC 3147 has hosted an extraordinary number of type Ia SNe relative to the theoretical prediction, and a normal numbers of type Ib/c and type II SN explosions. If one assumes the SNR values derived by Li et al. (2011), this issue is confirmed.

Table 1. Main parameters of SN 2008fv and its host galaxy.

Parent Galaxy	NGC 3147
Galaxy type	Sbc[1]
AGN class	Seyfert 2[2]
Redshift	0.009[1]
Velocity recession	3157 ± 22 km s^{-1}[1,*]
$RA_{Gal(J2000)}$	$10^h16^m53.65^s$[1]
$Dec_{Gal(J2000)}$	+73°24′02.695″[1]
Galaxy extinction	A_B = 0.104 mag[3]
	A_V = 0.080 mag[3]
$E(B-V)_{Gal}$	0.024 mag[3]

Notes. [1] NED (http://nedwww.ipac.caltech.edu); [*] corrected for LG onto Virgo + Shapley + Great Attractor infall Moore & Li (2004); [2] Hyperleda (http://leda.univ-lyon1.fr); [3] Schlegel et al. (1998).

A more precise evaluation of the stellar content of NGC 3147 is provided by Thöne et al. (2009), who calculate the SNR for a sample of ∼50 galaxies, including NGC 3147. Using the radio data of NGC 3147, they evaluates a total SNR of 0.18 SNe/yr, where 0.06 SNe/yr are type Ia, 0.09 are type Ibc, and 0.03 are type II. By using these values, our approximate computation implies that ∼2 SNe Ia, ∼3 SNe Ib, and only one SNe II are expected in NGC 3147 over a period of ∼40 years. These estimates appear to be in more satisfactory agreement with the number of SNe observed to date and suggest that the host galaxy of SN 2008fv is a normal "factory" of SNe Ia. Nevertheless, the ratio Ia/Ib foreseen by Thöne et al. (2009) is smaller than that obtained by observations of NGC 3147. These considerations have, of course, made carefully owing to the extremely low statistics.

2.2. Observations and data reduction

Our optical data have been obtained with the 0.72 m Teramo Normal Telescope (TNT) equipped with the E2V-CCD47-10 back-illuminated CCD camera, covering a field of view of 7 × 7 arcmin^2 with a pixel scale of 0.4″/pixel. Over several nights spanning from October 6 and December 9 2008, we obtained different sets of BVRI images of the SN field with a fairly good temporal sampling. These images were processed using standard bias subtraction and flat-fielding normalization technique, and the instrumental magnitudes were obtained by applying point-spread function (PSF) photometry on each image using the ROMAFOT package (Buonanno et al. 1979, 1983).

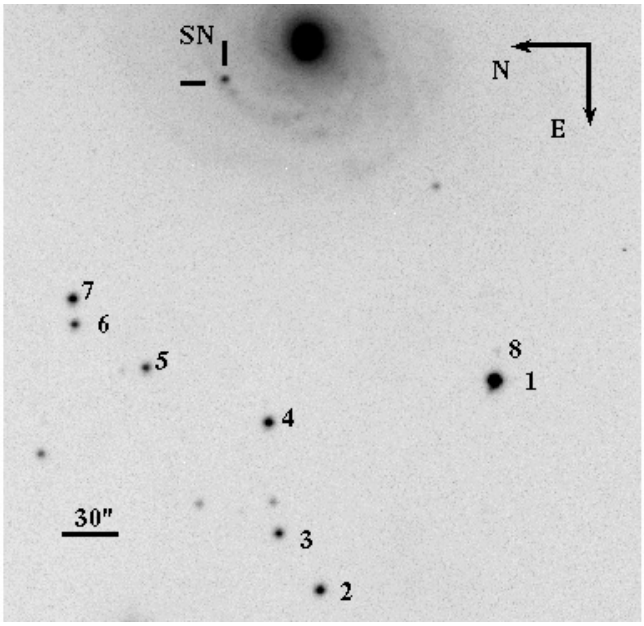

Fig. 1. *V*-band image of SN 2008fv in NGC 3147, obtained at the TNT telescope on JD+2453 760.5. The supernova and the 7 local reference stars are shown.

Table 2. Optical magnitudes for the local reference stars in the field of SN 2008fv.

Star	B (mag)	δB (mag)	V (mag)	δV (mag)	R (mag)	δR (mag)	I (mag)	δI (mag)
1	14.81	0.04	14.17	0.03	13.85	0.05	13.32	0.09
2	–	–	16.095	0.01	15.70	0.03	15.11	0.04
3	–	–	16.51	0.07	16.05	0.09	15.54	0.03
4	16.59	0.06	15.96	0.04	15.59	0.04	15.08	0.02
5	–	–	16.57	0.1	16.38	0.1	15.69	0.09
6	–	–	16.69	0.04	16.12	0.02	15.41	0.06
7	16.48	0.04	15.93	0.05	15.71	0.03	15.20	0.1

Since the SN lies in a region only marginally contaminated by the host-galaxy light, this background can be properly fitted by means of the specific capabilities of the ROMAFOT package. In particular, we select the tilted plane option to account for the gradient produced by the diffuse emission from the galaxy near the SN. With this choice, the background residuals (i.e., the original frame minus diffuse galaxy image) are minimized and the related uncertainties are included in the error budget of the photometric results.

As a consequence, the PSF magnitudes provide excellent measurements of the SN fluxes. In Table 2, we list the magnitudes of the local standards close to the SN position, as labeled in Fig. 1. These local standards are calibrated by using two nearby standard fields (Moffett & Barnes 1979; Oja 1996)[1], observed during the SN follow-up and during a calibration campaign performed about one year later. The NIR observations were carried out by using the AZT-24 telescope at Campo Imperatore (Italy) equipped with the NIR SWIRCAM camera (Brocato & Dolci 2003), which is based on a 256 × 256 HgCdTe NICMOS3 class array (PICNIC). The detector is sensitive to radiation in the spectral range from 0.9 to 2.5 μm and, at the focus of AZT-24,

[1] The tabulated R and I absolute magnitudes by Moffett & Barnes (1979) are given in the Johnson system. We transformed these magnitudes to the Cousins system adopting the relationships provided by Bessell (1979).

Table 3. NIR magnitudes for the local reference stars near SN 2008fv.

Star	J (mag)	δJ (mag)	H (mag)	δH (mag)	K (mag)	δK (mag)
1	12.78	0.03	12.49	0.08	12.4	0.1
2	–	–	–	–	–	–
3	14.80	0.01	14.49	0.01	14.5	0.1
4	14.40	0.02	14.00	0.07	13.96	0.08
5	15.12	0.03	14.75	0.04	14.8	0.1
6	14.68	0.05	14.17	0.02	14.1	0.1
7	14.91	0.03	14.55	0.05	14.5	0.1
8	15.56	0.03	14.96	0.07	14.8	0.1

yields a scale of 1.04″ pixel^{-1}, resulting in a field of view of 4.4 × 4.4 arcmin^2. The final scientific frames in these bands are obtained after performing a subtraction of the sky background, flat-fielding, the removal of bad pixels, and combining the dithered exposures. Infrared photometric observations began the October 09 and ended November 18 2008. As for the optical bands, the magnitudes of SN 2008fv are measured using PSF photometry. A series of NIR images of the standard star P035R (α(2000.0) = 08^{h}25^{m}43.8^s, δ(2000.0) = +73°01′18″, see Persson et al. 1998) were obtained to calibrate the same local photometric sequence adopted for the optical bands. The resulting magnitudes are listed in Table 3. To verify the reliability of our measurements, the calibrated magnitudes of the secondary standards are compared to the 2MASS catalog. Taking into account all the eight secondary stars, relatively small averaged differences are found of $\langle J_{\rm seq} - J_{\rm 2MASS}\rangle = 0.03 \pm 0.09$ mag, $\langle H_{\rm seq} - H_{\rm 2MASS}\rangle = 0.03 \pm 0.09$ mag, and $\langle K_{\rm seq} - K_{\rm 2MASS}\rangle = 0.03 \pm 0.06$ mag. The final optical and infrared photometry of SN 2008fv are presented in Tables 4 and 5. We performed a specific effort to evaluate the global uncertainties in our photometry for each filter. A set of star images with magnitudes quite similar to the SN are selected at each given epoch, subsequently these "artificial" stars are added to different regions of the original frame. Care is taken to include regions where the galaxy background is similar (or worse) than that observed in the actual SN area. The data reduction is then repeated. Thus, the rms of the PSF photometry of these artificial stars are adopted to provide a safe evaluation of the overall uncertainties affecting our photometry (excluding possible systematics caused by our calibrations) and this uncertainties are reported in the aforementioned tables for each band.

2.2.1. Photometric system characterization

We now briefly review some features, not presently available, of the instruments used to obtain NIR and optical images of the SN 2008fv follow-up. In particular, the transmission curves are shown in Fig. 2 by following the standard definition of the instrumental passband $S(\lambda)$

$$S(\lambda) = F(\lambda)QE(\lambda)A(\lambda)M(\lambda)L(\lambda), \quad (1)$$

where $F(\lambda)$ is the filter transmission, $QE(\lambda)$ is the detector quantum efficiency, $A(\lambda)$ is the atmospheric transmission, $M(\lambda)$ is the mirror reflectivity function, and $L(\lambda)$ is the lens throughput. The transmission curves of the NIR filters are provided by the engineering tests of the Infrared Laboratories Inc. where the camera was originally assembled, while transmission curves of the optical filters are derived directly at the optical laboratory of the Teramo Observatory. We adopt the quantum efficiencies reported by the original acceptance tests of the CCDs. For the

Table 4. Optical photometry of SN 2008fv.

Julian date (+2 453 000)	Epoch (days)	B (mag)	δB (mag)	V (mag)	δV (mag)	R (mag)	δR (mag)	I (mag)	δI (mag)
745.5[a]	–4.3	14.76	0.05	14.56	0.06	14.57	0.05	15.03	0.04
754.5	4.6	14.61	0.07	14.52	0.04	–	–	–	–
755.5	5.6	14.87	0.07	14.55	0.07	14.55	0.05	15.36	0.05
760.5[a]	10.6	15.25	0.05	14.86	0.03	14.94	0.04	15.68	0.03
761.5	11.6	15.35	0.09	–	–	–	–	–	–
769.5[a]	19.5	16.01	0.04	15.25	0.03	15.13	0.04	15.72	0.04
779.5	29.4	16.95	0.07	15.83	0.03	15.48	0.06	15.52	0.06
780.5	30.4	17.01	0.07	15.93	0.05	15.59	0.05	15.58	0.04
788.5	38.3	17.42	0.09	16.33	0.03	16.01	0.05 16.11	0.04	
800.5	50.2	–	–	16.72	0.05	16.41	0.05	16.68	0.05
807.5	57.1	17.72	0.07	16.92	0.05	16.66	0.06	17.11	0.05

Notes. Epochs are given with respect to the time of B-max and they are corrected for time dilation. [a] Photometric nights.

Table 5. NIR photometry of SN 2008fv.

Julian date (+2 453 000)	Epoch (days)	J (mag)	δJ (mag)	H (mag)	δH (mag)	K (mag)	δK (mag)
749.1[a]	–0.7	14.62	0.05	15.20	0.08	14.76	0.03
755.1	5.2	14.91	0.05	–	–	–	–
757.1[a]	7.2	15.61	0.03	15.30	0.05	15.06	0.05
759.1	9.2	15.65	0.08	15.26	0.08	15.21	0.08
760.1	10.2	15.91	0.09	–	–	–	–
761.1[a]	11.2	15.97	0.08	15.42	0.05	15.39	0.02
762.1	12.1	16.16	0.05	–	–	–	–
765.1	15.1	–	–	15.34	0.09	15.2	0.1
766.1	16.1	16.32	0.04	–	–	15.17	0.05
772.1[a]	22.1	15.85	0.05	15.03	0.04	14.88	0.03
773.1	23.0	15.85	0.03	15.03	0.02	14.88	0.03
779.1	29.0	15.61	0.08	15.00	0.08	15.09	0.08
780.1	30.0	15.48	0.07	14.99	0.06	15.00	0.05
781.1	31.0	15.51	0.09	15.0	0.1	15.10	0.15
787.1	37.0	15.78	0.05	15.37	0.05	15.43	0.05
789.1	38.9	16.00	0.05	15.48	0.05	15.58	0.05

Notes. Epochs are given with respect to the time of B-max and they are corrected for time dilation. [b] Photometric nights.

sake of simplicity, we take the CTIO atmospheric transmission curves available in IRAF[2] for the optical bands, while for the NIR we use a typical atmospheric transmission obtained under good weather conditions at Campo Imperatore. The mirror reflectivity function was obtained using a standard aluminum reflectivity curve. Finally, for all the bands we assume that the lens throughput is constant across the whole spectral range. The comparison between the BVRI photometric system adopted in this work and the standard Johnson-Cousins system is shown in Fig. 2. In the same figure, we also present a similar comparison for the NIR bands. Tables 6 and 7 list the data plotted in Fig. 2. The differences are typically taken into account using the calibration procedure based on a well observed set of standard stars.

The main concern is probably the relatively small blue leak found in shape of the TNT V, R, and I bands. To evaluate the effect of this unwanted feature on the photometric measurements, we perform specific tests taking advantage by the SYNPHOT which is available on IRAF package. The expected magnitudes for each band of the two (our & standard) photometric systems

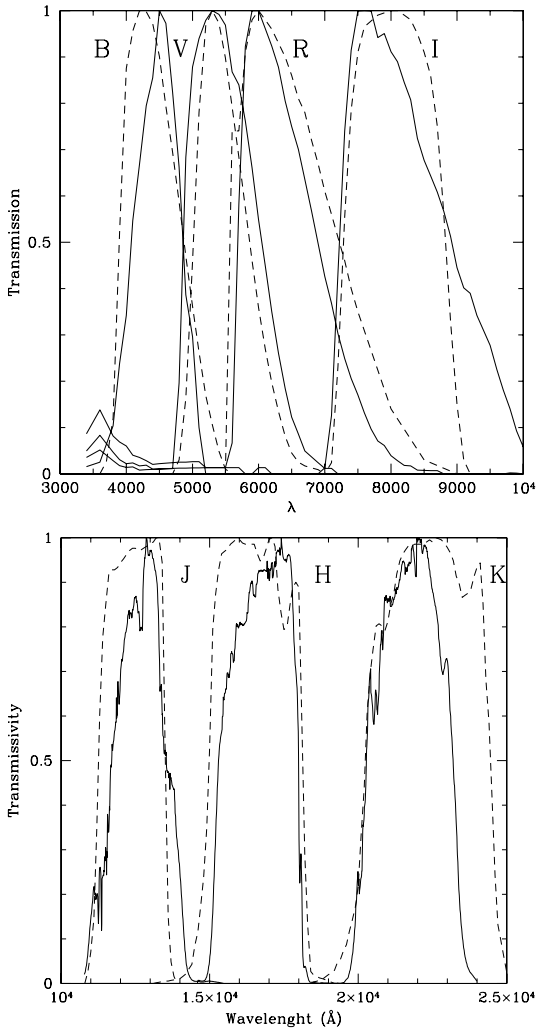

Fig. 2. *Upper panel*: The BVRI transmission curves, normalized to the peak transmission (solid line), compared with the standard Bessell (1990) BVRI filter (dashed line). *Lower panel*: the JHK transmission curves, normalized to the peak transmission (solid line). As reference, we also plot the Persson et al. (1998) JHK filter curves (dashed line).

are derived by assuming the same input spectral energy distribution (SED). In particular, we use *i*) SN spectral template provided by Hsiao et al. (2007) and *ii*) several S,ED obtained from the Kurucz atmosphere stellar models having different temperatures and chemical compositions. As a result, we find that the

[2] IRAF is distributed by the National Optical Astronomy Observatories, which are operated by the Association of Universities for Research in Astronomy, Inc., under cooperative agreement with the National Science Foundation.

difference between the magnitude measured with a standard filter Johnson (1965), Bessell (1979, 1990), and the TNT V, R, I filters are smaller than the photometric uncertainties adopted in the present work for our photometric results. As a further check, we evaluate the uncertainties specifically caused by the blue leak in the transmission curves of the TNT bands. We artificially smooth to negligible throughput values the TNT transmission curves (VRI) across the wavelengths interval 3500−4500 Å, i.e. where the blue leak is found. It turns out that the new magnitudes, computed with this "modified" transmission curves, differ from the previous ones of values much smaller than 0.01 mag. In conclusion, we find that these blue leaks in the TNT VRI filters do not affect our photometric results, at least within the given photometric uncertainties, and can be considered negligible for the purpose of this paper. Similar tests involving the NIR bands show that the uncertainties caused by the adopted filters are at most of the order of ∼0.05 mag.

2.2.2. The K-correction

The redshift of the host galaxy of SN 2008fv appears (Table 1) to be sufficiently low to have no significant effect on the observed magnitudes. Nevertheless, we compute the K-correction to modify our photometry to the rest frame and, as a consequence, to properly compare the intrinsic luminosities and colours of different SNe Ia.

The SN SED is needed to achieve this goal (Leibundgut 1990; Hamuy et al. 1993; Nugent et al. 2002; Hsiao et al. 2007). Briefly, we recall that the K term correction at an effective wavelength λ_i in the X band can be written as

$$K_i(\lambda) = 2.5\log(1+z) + 2.5\log\frac{\int F(\lambda)\,S_i(\lambda)\,\mathrm{d}\lambda}{\int F[\frac{\lambda}{(1+z)}]\,S_i(\lambda)\,\mathrm{d}\lambda}, \quad (2)$$

where $F(\lambda)$ is the observed specific flux of the supernova, and $S_i(\lambda)$ is the total passband transmission, given by Eq. (1).

In the absence of spectral observation of SN 2008fv, we assumed the spectral template provided by Hsiao et al. (2007) and obtained as the combination of about 1000 observed spectra of ∼100 SNe. We adopted the specific response curves of our photometric system, both in optical and in the infrared. As a result, the K-corrections are reported in Tables 8 and 9, respectively. We note that they are typically below ∼0.03 in the optical bands and below ∼0.07 in the NIR ones. This confirms that the effect of the redshift on the photometric measurements of SN 2008fv is fairly small.

3. Result and analysis

3.1. Optical and near-IR light curves

The BVRI LCs of SN 2008fv are presented in the lower part of Fig. 3, where it is shown that our optical photometry covers the pre-maximum phase until two months after maximum. The time and the magnitude at maximum light are estimated via a third-order polynomial fits to the data around the peaks or a spline interpolation when only a few points are available, i.e. in the R- and I-bands. The fit is performed by including the data from the first available epoch before the maximum up to ten days after it. From the results, provided in Table 10, it is evident that the V- and R-band peaks are delayed with respect to the B-band maximum (B-max) of ∼1.5 days and ∼1.7 days, a feature already known from other well-studied SN Ia (e.g., Hamuy et al. 1996b). Moreover, the I-band maximum occurs at about ∼1.8 days before it. From the estimated B-band peak magnitude ($B_{\max}$ = 14.55 ± 0.05 mag on JD+2 454 749.8, corrected for a Galactic extinction value of $E(B-V)$ = 0.024 mag by Schlegel et al. 1998), we derive a decline rate $\Delta m_{15}(B)$ = 0.94 ± 0.05 mag (the magnitude at +15 days is derived by interpolating the nearest photometric points). This result is supported by the comparison of SN 2008fv LCs with the observed LCs of SNe that have

Table 8. K-correction to be added to the optical magnitudes of SN 2008fv.

Julian date (+2 453 000)	Epoch[a] (days)	B (mag)	V (mag)	R (mag)	I (mag)
745.5	–4.3	0.019	0.010	0.020	0.0152
754.5	4.7	0.005	0.003	0.023	0.0067
755.5	5.7	–0.018	–0.006	0.012	–0.001
760.5	10.7	–0.019	–0.009	0.013	–0.0002
761.5	11.7	–0.020	–0.019	0.010	–0.005
769.5	19.7	–0.027	–0.020	0.014	–0.006
779.5	29.7	–0.018	–0.019	0.020	0.005
780.5	30.7	–0.019	–0.019	0.020	0.004
788.5	38.7	–0.018	–0.010	0.019	0.007
800.5	50.7	0.013	0.005	0.017	0.012
807.5	57.5	0.012	0.004	0.016	0.012

Notes. [(a)] Epochs are given with respect to the time of B-max. Epochs are corrected for time dilation.

Table 9. K-correction to be added to the NIR magnitudes of SN 2008fv.

Julian date (+2 453 000)	Epoch[a] (days)	J (mag)	H (mag)	K (mag)	(mag)
749.1	–0.7	0.024	0.011	0.032	
755.1	5.3	0.026	–0.011	0.052	
757.1	7.3	0.029	–0.013	0.053	
759.1	9.3	0.034	–0.015	–0.033	
760.1	10.3	0.036	–0.020	–0.043	
761.1	11.3	0.037	–0.021	0.062	
762.1	12.3	0.039	–0.022	0.063	
765.1	15.3	0.047	–0.024	0.050	
766.1	16.3	0.048	–0.027	0.052	
772.1	22.3	0.056	–0.026	0.041	
773.1	23.3	0.064	–0.022	0.035	
779.1	29.3	0.070	–0.014	0.014	
780.1	30.3	0.069	–0.008	0.010	
781.1	31.3	0.068	–0.002	0.006	
787.1	37.3	0.073	0.019	0.016	
789.1	39.3	0.070	0.017	0.016	

Notes. [(a)] Epochs are given with respect to the time of B-max. Epochs are corrected for time dilation.

Table 10. Best fit parameters for the apparent maximum magnitudes and Julian Date at maximum in all bands.

Band	Julian date at maximum (+2 453 000)	Magnitude at maximum. (mag)
B	749.8 ± 0.2	14.55 ± 0.05
V	751.1 ± 0.5	14.38 ± 0.05
R	751.3 ± 0.5	14.40 ± 0.05
I	748.0 ± 0.5	14.53 ± 0.05
J	746.2 ± 0.5	14.81 ± 0.07
H	746.2 ± 0.5	15.12 ± 0.08
K	747.5 ± 0.5	14.89 ± 0.08

Notes. The data are corrected for the Galactic extinction by using the Cardelli et al. (1989) law.

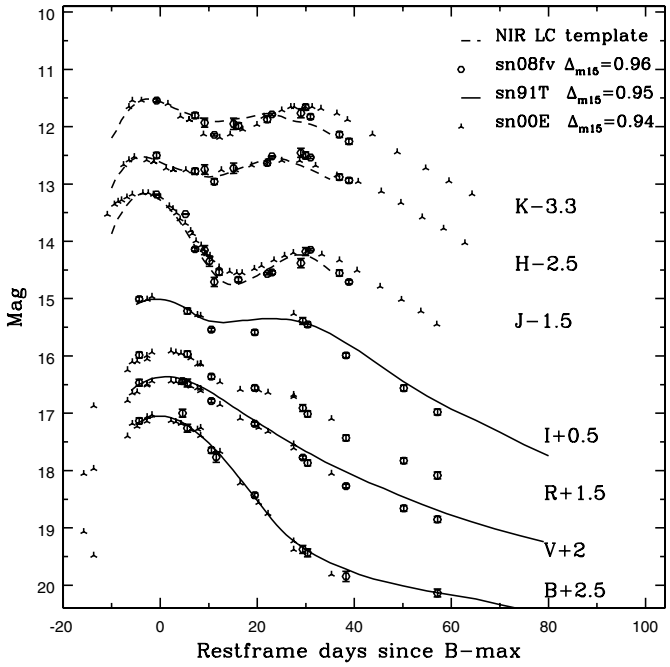

Fig. 3. Optical and infrared LCs of SN 2008fv (open circle) compared with those of SN 2000E (starred triangles, UBVRIJHK bands), SN 1991T (solid line, only in the optical bands), and the NIR template provided by Wood-Vasey et al. (2008) (dashed line, only in the NIR bands). The phase is measured in days from the B maximum and the LCs of SNe used for the comparison are vertically shifted in order SN 2008fv that data of at maximum.

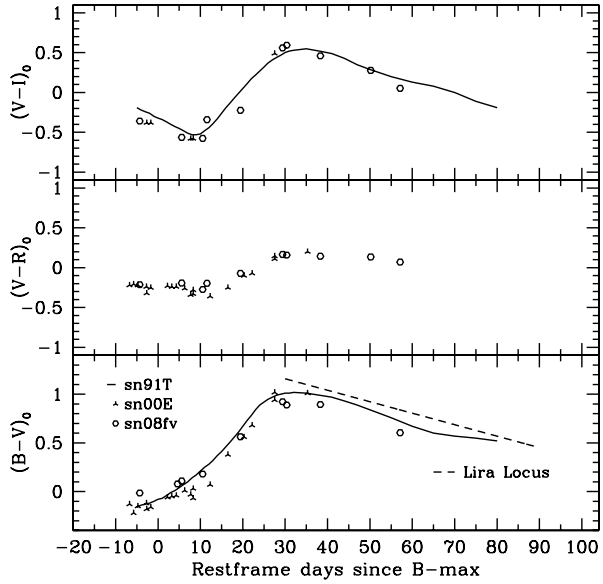

Fig. 4. The $(B-V)_0$, $(V-R)_0$ and $(V-I)_0$ colour curves of SN 2008fv, corrected for the Galactic reddening (Cardelli et al. 1989) S law and $R_V = 3.1$ and for the host galaxy reddening with $R_V = 2.9$ (see Sect. 3.2 for details). The colour curves of labeled SNe, corrected for their respective colour excess, are also show. The Lira (1995) relation (dashed line) predicts a lower $E(B-V)$ than derived from the maximum light and adopted as the "*true*" host galaxy reddening (see text). As a consequence, the Lira relation does not provide a good fit of the dereddened colour curves.

similar $\Delta m_{15}(B)$ values, such as SN 2000E (Valentini et al. 2003, $\Delta m_{15}(B) = 0.94$) and the LC templates of SN 1991T (Hamuy et al. 1996a, $\Delta m_{15}(B) = 0.95$). As shown in Fig. 3 SN 2008fv is very similar to SN 2000E in all bands and also to SN 1991T in B and V, and to a lower degree in I. In the upper part of Fig. 3, we present the JHK LCs of SN 2008fv where the characteristic double-peaked morphology of the NIR bands can be clearly seen. In the pre-maximum phases, the NIR photometric coverage is more incomplete than the optical one, our NIR observations indeed beginning on JD+2 454 749.1, i.e. close to the B-max epoch. As a consequence, no data are available before the infrared maximum. Nevertheless, it is possible to constrain the SN 2008fv maximum brightness, and its epoch, by using the infrared light curves templates provided by Wood-Vasey et al. (2008), which are based on a homogeneous sample of 18 PAIRTEL SNe Ia LCs. In the NIR bands, the best fit results are reported in Table 10: the band maximum light occurs 3.6 (J), 3.6 (H) and 2.8 (K) days before the B-max. The secondary maximum takes place at ~JD+2 454 779.1 in J-band and ~JD+2 454 778.1 in the H- and K-band, i.e. ~32–33 days since B-max.

3.2. Optical and near-IR colour curves

We present the $(B-V)_0$, $(V-R)_0$ and $(V-I)_0$ colour curves of SN 2008fv in Fig. 4 together with the colour curves of SN 2000E and SN 1991T. As described at the end of this section, our data are corrected by "Galaxy + host" reddening, i.e. we assume the appropriate value of $E(B-V)_{\rm Gal}$ from Schlegel et al. (1998) with $R_V = 3.1$ and $E(B-V)_{\rm host} = 0.22$ with $R_V = 2.9$. Moreover, the Cardelli et al. (1989) law is used.

As already shown in the previous section, the LCs of SN 2008fv and those of SN 2000E are very similar, thus it is unsurprising that the shape of their colour curves are almost comparable. Thus, within the limits of the relatively poor sampling, the $(B-V)_0$ colour appears to increase by moving from the time of the first NIR peak up to that of the NIR minimum. This evolution toward red colours proceeds, with a different (steeper) slope, until the epoch of the secondary NIR maximum, when it reaches a maximum. Afterwards, the $(B-V)_0$ decreases linearly. As already pointed out by Lira (1995), this trend was visible for SNe Ia with $0.85 < \Delta m_{15}(B)({\rm mag}) < 1.9$ from 30 to 90 days after V maximum. As a consequence, the $(B-V)$ can be used as reddening indicator by evaluating the offset between the $(B-V)$ data of SNIa in this epoch range and the Lira relation (Lira 1995). In the case of SN 2008fv, we find that $E(B-V)_{\rm tail} = 0.08 \pm 0.05$ mag.

An independent method to derive the host galaxy reddening was first proposed by Phillips et al. (1999), by using the correlation between the light-curve width parameter Δm_{15} and the intrinsic $B_{\rm max}-V_{\rm max}$ value (or the $V_{\rm max}-I_{\rm max}$). Using this correlation to estimate the host galaxy reddening of SN 2008fv, we find that $E(B-V)_{\rm max} = 0.22 \pm 0.05$ mag, which is inconsistent with the reddening value obtained from the relations involving the Lira relation. Since the two colour excesses are derived at different epochs of the colour evolution, small systematics in the two different estimates of $E(B-V)$ are expected. Nevertheless, Folatelli et al. (2010) find differences in the $E(B-V)_{\rm tail}$ and $E(B-V)_{\rm max}$ that are similar to the ones obtained in this work but, they also demonstrate that the expected systematic differences are smaller than the observed ones. The origin of this behavior is poorly understood, however, the existence of this discrepancy suggests that a component in one or other of the two $E(B-V)$ values is not due to the host dust. Therefore, we take advantage of the availability of data spanning from the B to the K bands to shed light on the $E(B-V)$

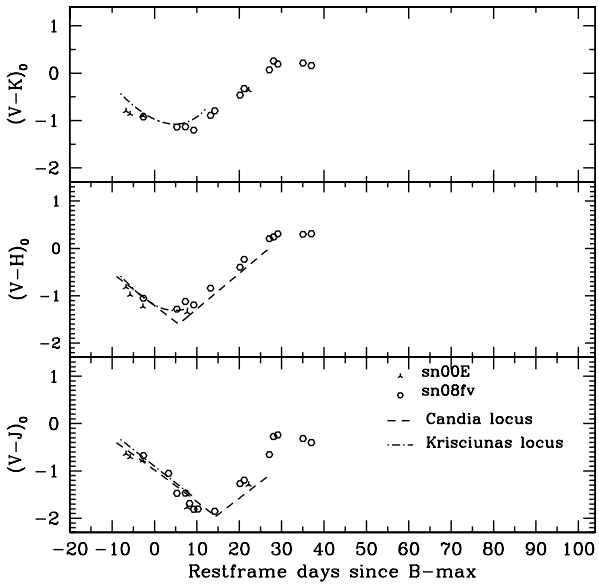

Fig. 5. $(V-J)_0, (V-H)_0$ and $(V-K)_0$ colour curves of SN 2008fv are plotted with the ones of the SN2000E. All data are corrected for the total Galactic+host reddening), by assuming the proper value for R_V (see text). The NIR loci predicted by Candia et al. (2003) and Krisciunas et al. (2004c) are also plotted as dashed and dot – short dashed lines.

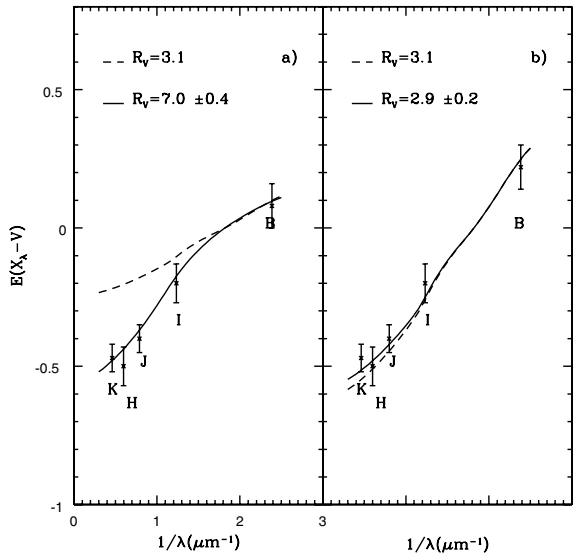

Fig. 6. Colour excesses $E(V-X_\lambda)$ for bands X_λ = BVIJHK for SN 2008fv. In panel **a)**, the solid line represents the best fit of the data for $R_V = 7.0$, when $E(B-V)_{\rm tail}$ is used. In panel **b)**, adopting $E(B-V)_{\rm max}$, the best fit is achieved with $R_V = 2.9$. In both panel, the dashed line shows the standard extinction law with $R_V = 3.1$.

Table 11. NGC 3147 colour excess as derived using several method.

Direct measurements	
$E(B-V)_{\rm tail}$	0.08 ± 0.05
$E(B-V)_{\rm max}$	0.22 ± 0.05
$E(V-I)_{\rm max}$	0.20 ± 0.07
$E(V-J)$	0.40 ± 0.05
$E(V-H)$	0.50 ± 0.07
$E(V-K)$	0.45 ± 0.05

discrepancies we have found. First at all, we derive the colour excesses in all the available bands, as listed in Table 11. The $(V-I)$ colour excess has been derived from the maximum light colours (Phillips et al. 1999), while the colour excesses in the $(V-$ NIR) bands were obtained using the observed $(V-J)$, $(V-H)$ and $(V-K)$ colours of SN 2008fv, shown in Fig. 5. The V minus NIR colours of SNe Ia are quite uniform around B maximum light. It has been demonstrated that they can be considered as a reddening estimator that is more reliable than colours obtained in the optical wavelengths (Krisciunas et al. 2007). By adopting the $(V-$ NIR) loci provided by Candia et al. (2003, hereafter C03) for the slow declining SNe, we obtain $E(V-J) = 0.40 \pm 0.05$, $E(V-H) = 0.50 \pm 0.07$ mag. These results do not significantly differ when Krisciunas et al. (2004c, hereafter K04) loci are also assumed. A reddening of $E(V-K) = 0.45 \pm 0.05$ is found using the K04 template.

When we then assume that the dust extinction in the host galaxies obeys the law introduced by Cardelli et al. (1989), we investigate which value of the absorption coefficient R_V is favorable to SN 2008fv. Cardelli et al. (1989) provide an analytic expression for the average extinction law, $A_\lambda/A_V = a_\lambda + b_\lambda/R_V$, where a_λ and b_λ are wavelength-dependent coefficients (see their Eqs. (2) and (3)). We plot in Fig. 6 the colour excess (BVIJHK minus V) versus the effective wavelength, using both $E(B-V)$ values. When the $E(B-V)_{\rm tail}$ is adopted (see panel **a)**), the best fit of the data is achieved with $R_V = 7.0 \pm 0.4$, which lies beyond the range of values measured for the Milky Way (see Valencic et al. 2004). In the panel **b)** of the figure, the same fit is repeated by assuming the $E(B-V)_{\rm max}$. In this case, the best value of R_V is 2.9 ± 0.2 which agrees (within the errors) with the averaged value of $R_V = 3.2 \pm 0.4$ derived by Folatelli et al. (2010) for a sample of 13 SNe with low and moderate reddening. Thus, in the following analysis, we assume that the $E(B-V)_{\rm max}$ value, with $R_V = 2.9 \pm 0.2$, is the most reliable for the host galaxy reddening, $E(B-V)_{\rm host}$.

3.3. The distance to NGC 3147 and the luminosity of SN 2008fv

Once the evaluation of the total reddening $E(B-V)$ is available, we can estimate the $\Delta m_{15}(B)_{\rm true}$ corrected by reddening as

$$\Delta m_{15}(B)_{\rm true} = \Delta m_{15}(B)_{\rm obs} + 0.1 \cdot [E(B-V)_{\rm Gal} + E(B-V)_{\rm host}], \quad (3)$$

(Phillips et al. 1999). In this way, the $\Delta m_{15}(B)$ become 0.96 ± 0.08, and SN 2008fv could be included in the class of slow-declining SNe. This class of SNe can be spectroscopically peculiar before B-max in a similar way to SN 1991T or almost normal as for SN 1999aa (Hamuy et al. 2002). In both cases, they lie at the bright end of the luminosity distribution, which are ∼0.3 mag larger than the normal ones (Wang et al. 2006, see their Fig. 5). Unfortunately, for SN 2008fv spectral observations are unavailable, thus we are unable to use this method to determine its nature (SN 1991T-like or SN 1999aa like), although, as we previously noted, a week before the maximum, the spectrum of the SN 2008fv was classified as normal. Nevertheless, it should be mentioned that the SN appears as an unknown type in the CfA list[3]. As a consequence, the spectroscopic classification of SN 2008fv remains uncertain.

However, constraints on the absolute magnitude of SN 2008fv can be obtained. As a first step, we determine a distance

[3] http://www.cbat.eps.harvard.edu/lists/Supernovae.html

Table 12. Decline-rate corrected absolute B, V, R, I, J, H, and K magnitudes obtained by using various methods (see text).

Method	$M_{B,\max}$	$M_{V,\max}$	$M_{R,\max}$	$M_{I,\max}$	$M_{J,\max}$	$M_{H,\max}$	$M_{K,\max}$
Altavilla et al. (2004)[1]	-19.56 ± 0.07	–	–	–	–	–	
Prieto et al. (2006)[1]	-19.39 ± 0.08	-19.34 ± 0.08	-19.32 ± 0.1	-19.11 ± 0.09	–	–	–
Reindl et al. (2005)[2]	-19.27 ± 0.06	-19.25 ± 0.06	–	-18.96 ± 0.06	–	–	–
Wang et al. (2005, 2006)[3]	-19.40 ± 0.08	-19.31 ± 0.07	–	-19.02 ± 0.07	–	–	–
Folatelli et al. (2010)[4]	-19.29 ± 0.11	-19.25 ± 0.11	–	–	-18.53 ± 0.09	-18.25 ± 0.18	-18.42 ± 0.29
Folatelli et al. (2010)[2]	-19.33 ± 0.09	–	–	–	-18.60 ± 0.09	–	–
Folatelli et al. (2010)[5]	–	–	–	–	-18.44 ± 0.09	-18.42 ± 0.08	-18.47 ± 0.12
Krisciunas et al. (2004c)[5]	–	–	–	–	-18.61 ± 0.03	-18.28 ± 0.03	-18.44 ± 0.03
Weighted avg. $M_{\rm ave}$	-19.4 ± 0.1	-19.3 ± 0.1	-19.32 ± 0.1	-19.0 ± 0.1	-18.55 ± 0.08	-18.32 ± 0.09	-18.44 ± 0.03
Distance Modulus	33.1 ± 0.1	33.0 ± 0.1	33.3 ± 0.1	33.2 ± 0.1	33.2 ± 0.1	33.3 ± 0.1	33.30 ± 0.09
$\langle\mu\rangle_w = 33.2 \pm 0.1$							

Notes. All magnitudes are scaled to $H_0 = 72\,{\rm km\,s^{-1}\,Mpc^{-1}}$. The weighted averages of different estimates are also reported along with the statistical errors. These values are used to derive the distance modulus for each band and, finally, averaged to obtain a more robust estimate of μ. [1] Calibration using decline rates, without metallicity correction. [2] Relations to $M_{\rm max}$ versus $\Delta m_{15}(B)$ and colour. [3] Relations between Peak Luminosity and Color Parameter ΔC_{12}. [4] Calibration using decline rates and extinction. [5] Absolute magnitude at peak without any correction.

to the host galaxy using the calibrations of peak absolute magnitude available in the literature for all bands. The resulting absolute magnitudes at peak are listed in Table 12 in terms of different relationships between the absolute magnitude at peak, the decline rate and other LC properties, such as the colour for the Reindl et al. (2005) calibration or the reddening for the Folatelli et al. (2010) calibrations. In the NIR, we take advantage of the absolute magnitude at peak obtained by Krisciunas et al. (2004c) and Folatelli et al. (2010).

Since different methods have zero-points based on an inhomogeneous set of Hubble constant values, all absolute magnitudes are scaled to $H_0 = 72\,{\rm km\,s^{-1}\,Mpc^{-1}}$. The inspection of the absolute magnitudes at peak in the optical bands leads to the conclusion that the corrected peak luminosity of SN 2008fv is indistinguishable, within the uncertainties, from that of the mean of the normal SNe Ia (Wang et al. 2006). We also note that SN 2008fv is less luminous of ∼0.1 mag than SN 2000E. Therefore, SN 2008fv can be classified as a "slow declining" SN based on its Δm_{15}, having a luminosity that is at the lower end of the observed range of over-luminous SNe and close to the luminosity of normal SNe, as already observed for other slow-declining SNe (e.g., SN 1999aw Strolger et al. 2002).

Moreover, by means of the absolute peak magnitudes we also provide in Table 12 an evaluation of the μ in each band and an average value of 33.2 ± 0.1 mag, where the quoted error is statistical. This distance is in good agreement with $\mu = 33.1 \pm 0.1$ obtained by averaging all literature data of the host galaxy NGC 3147 found in the NED Redshift Independent Distance database[4].

3.4. Bolometric behaviour of SN 2008fv

To study the bolometric behaviour of SN 2008fv, all measurements in the BVRIJHK bands are dereddened using the reddening values of $E(B-V)_{\rm Gal} = 0.02$ and $E(B-V)_{\rm host} = 0.22$, with the proper R_V (3.1 and 2.9, respectively). The SN magnitudes are converted into fluxes using the zero-points in each bands calculated by means of the absolute fluxes for a zero-magnitude source provided by Bessell (1990) for the optical filters and Tokunaga & Vacca (2005) for the NIR ones. The resulting zero-points are listed in Table 13 along with the tabulated flux for a zero-magnitude star and the effective wavelengths of the employed photometric system.

Table 13. Filter, effective wavelength for the filter, mean flux density, and zeropoint magnitude for a zero magnitude source.

Band	Effective wavelengths (Å)	Flux F_λ (erg s^{-1} cm^{-2} Å^{-1})	ZP $= -2.5 \log F_\lambda$ (mag)
B	4374.5	63.2	20.5
V	5408.3	36.3	21.1
R	6201.8	21.8	21.6
I	8098.5	1.13	22.4
J	12680	3.01	23.8
H	16706	0.12	24.9
K	21662	0.04	26.0

Thus, we determine the bolometric luminosity as the area of trapezium connecting the BVRIJHK points (Valentini et al. 2003), and we assume the average distance modulus derived in this work. To correct the bolometric LC for missing data in the U passband, we set the flux to zero at 3000 Å and extrapolate the flux at 3600 Å (see Suntzeff 1996). We model the curve of the bolometric luminosity by using the results of spline fits to the LCs to ensure that we have homogeneous sets of magnitudes at all wavelengths for each epoch. Table 14 lists the *uvoir* bolometric luminosity of SN 2008fv and Fig. 7 shows its time evolution, the resulting LC is also compared with that of SN 2000E. According to the figure, it is clear that SN 2008fv is intrinsically fainter than the SN 2000E. Moreover, a secondary hump is clearly visible around ∼25−30 days, which we recall corresponds both to the V-band inflection point and the secondary maximum observed in the RIJHK bands. This feature is thought to appear in the IR-window as a consequence of the rapidly changing time dependence of the mean opacity (Pinto & Eastman 2000a,b; Kasen 2006).

By following Arnett (1982) and Stritzinger & Leibundgut (2005), we estimated the radioactive mass of ^{56}Ni from the maximum bolometric luminosity and the rise time $t_{\rm r}$ of the light curve, i.e, the time spent by the SN from the explosion to the B-maximum. A method to derive the rise time was proposed by

[4] For a complete list of methods, and associated references, visit the URL http://ned.ipac.caltech.edu/forms/d.html.

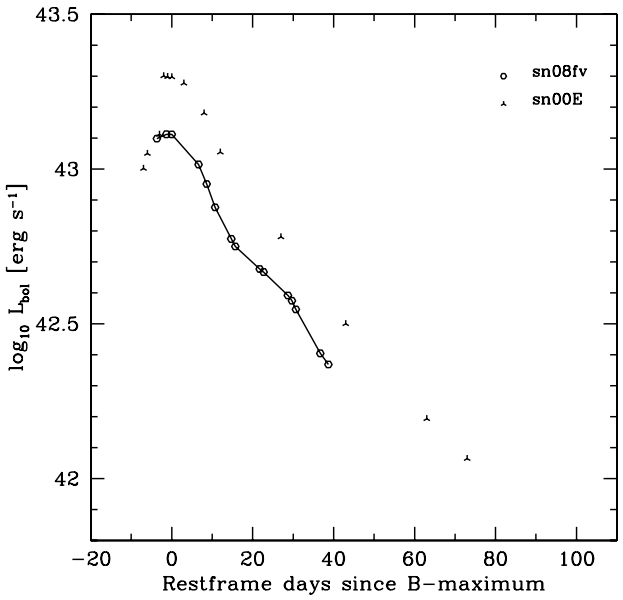

Fig. 7. The bolometric (*uvoir*) light curve for SN 2008fv (*open circles*). For the sake of comparison, the bolometric light curve of SN 2000E (*starred triangles*) is also plotted.

Table 14. Bolometric (uvoir) luminosities of SN 2008fv.

Julian date (+2 453 000)	Epoch (days)	Bolometric luminosity (10^{43} erg s^{-1})
745.5	–4.3	1.26
749.1	– 0.7	1.29
749.8	0.0	1.29
756.5	6.65	1.02
758.5	8.65	0.89
760.5	10.7	0.76
764.5	14.7	0.59
765.5	15.7	0.56
771.5	21.7	0.48
772.5	22.7	0.47
778.5	28.7	0.39
779.5	29.7	0.37
780.5	30.7	0.35
786.5	36.7	0.25
788.5	38.7	0.23

Riess et al. (1999), who suggested that at very early time the SNe Ia are homologous expanding fireballs, where the luminosity is roughly proportional to the square of the time since the explosion

$$L \propto (t + t_r)^2 , \quad (4)$$

where t_r is the rise time and t is the elapsed time relative to the maximum. To proceed with this argument we assumed that the earlier photometric data points SN 2000E in the R band are a reliable template of SN 2008fv. Under this hypothesis and by adopting the average distance modulus derived in the Sect. 3.3, we found that SN 2008fv exploded 20.6 days before the R-band maximum. This corresponds to a rise time in the B-band $t_r \sim 19.1 \pm 0.2$ days. This value is slightly shorter than the average rise time (~21.4 days) derived by Riess et al. (1999) for SNe with a similar value of $\Delta m_{15}(B)$, while it lies in the range of t_r observed for SNe with similar Δm_{15}, as found by the analysis of Ganeshalingam et al. (2011). On the basis of this evaluation of the rise time and by adopting the peak value of our *uvoir* bolometric LC, we find a ^{56}Ni mass of 0.7 ± 0.2 $M_\odot$. We note that this result agrees very well with a different and independent way of estimating the ^{56}Ni mass. The empirical relation between the decline rate Δm_{15} and the value of $M_{\rm Ni}$ (see e.g., Mazzali et al. 2007) gives $M_{Ni} = 0.7 \pm 0.1$.

4. The second maximum in the near-infrared

One of the most intriguing characteristic of the LCs of type Ia SNe is the secondary maximum in the near-infrared. The models of Kasen (2006) show that the timing and the prominence of secondary maximum are related to the iron-peak elements and to the ^{56}Ni mass. In this case, the timing and the prominence of this secondary maxima are expected to also be related to the value of Δm_{15}, just because this last quantity has shown a dependence on the Ni mass observed in the ejecta (e.g., Arnett 1982; Mazzali et al. 2007). Bearing this interdependences in mind, we used the Δm_{15} parameter to investigate the existence of possible correlations between the properties of the secondary maximum in the JHK bands and the optical properties. For the I-band, a similar analysis was already performed by Elias-Rosa et al. (2008) and Folatelli et al. (2010).

As a first step in this investigation, we compiled a data-set of 40 SNeIa, including SN 2008fv and SN 2000E. The selection criteria are based mainly on the availability in the literature of the following quantities: i) well sampled JHK-band LCs; ii) independent distance estimates; and iii) $\Delta m_{15}(B)$ ranging from 0.9 to 1.8. The result is summarized in Table 15, where we list some relevant quantities of the selected SNe, namely: the phase of the secondary maximum, $t_{2,X}$, where X is the filter, i.e. J, H or K-band; the absolute magnitude of primary maximum, $M_{1,X}$; the absolute magnitude of secondary maximum, $M_{2,X}$; the absolute magnitude of local minimum $M_{0,X}$; and the decline rates $\Delta m_t(X)$ measured from the LCs in the X-band as the difference between the t rest-frame days since maximum light in that band and the peak magnitude. The $M_{1,X}$, $M_{2,X}$, and $M_{0,X}$ values are derived from the observed light curves, performing polynomial fits of data near the considered epoch (i.e., $t_{1,X}$, $t_{2,X}$ and $t_{0,X}$, respectively). The reader can notice that only a few fast declining SNe are presented in the table, two of them have $\Delta m_{15} \sim 1.8$. As already pointed-out by Hamuy et al. (1996a), this low quality of the data statistic appears to be caused by the weakness of the second peak of the fast declining and its blending with the principal peak. In particular, the two fast declining SNe with $\Delta m_{15} \sim 1.8$ in the selected SN sample do not have secondary hump in the H and K-band. Moreover, Krisciunas et al. (2009) observed that the fast declining peaking after the B-band maximum each have an extremely weak (or no) secondary peak in the NIR bands. For these reason, we do not include in our sample the fast declining SNe that peak after the B-max, with the exception of SN 2005ke which peaks only one days after the B-max and shows a weak but recognizable secondary maximum in the J-band.

A first result of our analysis is that we identify the presence of a correlation, with a large Pearson coefficient, between $t_{2,X}$ and the $\Delta m_{15}(B)$ in all the JHK-band. This is shown in the lower panels of Fig. 8. On the other hand, no correlation is found between the absolute magnitude of the secondary peak, $M_{2,X}$ and $\Delta m_{15}(B)$ (upper panels of the same figure). Both these behaviours were predicted qualitatively by Candia et al. (2003, see their Fig. 7) and Krisciunas et al. (2004b), although several exceptions have been reported (e.g., SN 2000cx Candia et al. 2003). Thanks to the data-set we collected, we were able

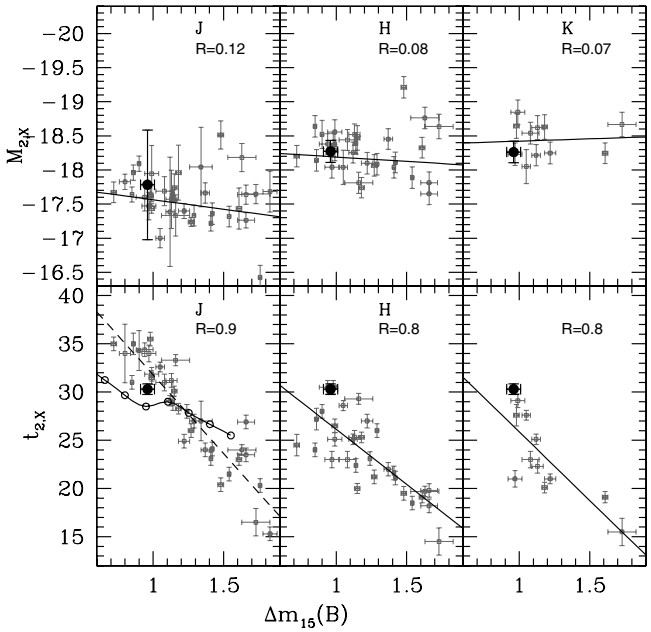

Fig. 8. The time since B maximum of secondary NIR peak (*lower panel*) and the absolute magnitude of secondary peak (*upper panel*) versus the $\Delta m_{15}(B)$. SN 2008fv is represented with large circles, the data from literature with small open squares. The Pearson coefficients R is also shown for each panel with the resulting best fit of data (*solid line*). For the timing of secondary maximum in J-band, we also plot the prediction of Kasen (2006) models (*solid line and open circles*).

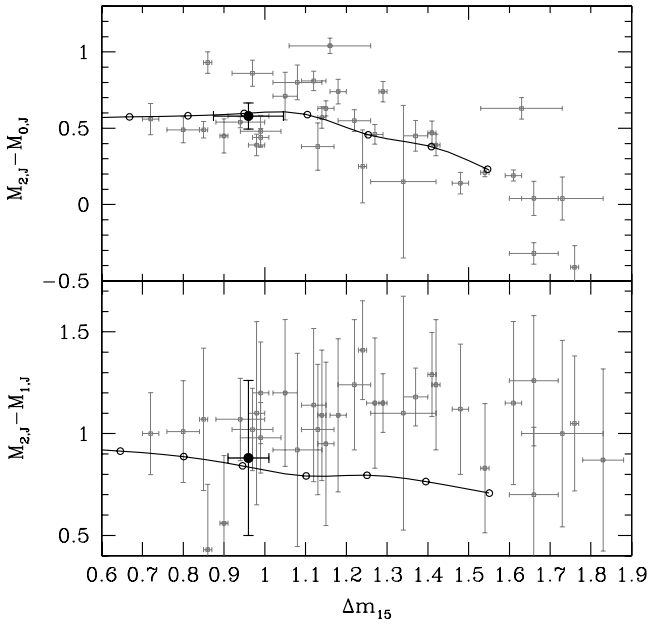

Fig. 9. Strength of the secondary maximum in the J-band as a function of the decline rate $\Delta m_{15}(B)$. The symbols are the same as in Fig. 8. The lower panel shows the difference in magnitudes between the secondary maximum and the primary maximum, while the upper panel displays the difference in magnitudes between the secondary maximum and the local minimum. In each panel, the same quantities predicted by Kasen (2006) models are plotted for comparison.

to derive the set of relationships between t_2 measured in the NIR bands and $\Delta m_{15}(B)$, given by

$$t_{2,J} = (30.0 \pm 2.0) + (-16.2 \pm 1.2) \cdot [\Delta m_{15}(B) - 1.1], \quad (5)$$
$$\text{rms} = 2.0 \text{ days}$$
$$t_{2,H} = (25.0 \pm 2.7) + (-12.9 \pm 1.7) \cdot [\Delta m_{15}(B) - 1.1], \quad (6)$$
$$\text{rms} = 2.5 \text{ days}$$
$$t_{2,K} = (24.4 \pm 5.5) + (-14.2 \pm 3.5) \cdot [\Delta m_{15}(B) - 1.1], \quad (7)$$
$$\text{rms} = 3.0 \text{ days}.$$

Owing to the relatively small number of available observational data (particularly in the K-band), the coefficients of the equations need to be improved. Thus, to derive more robust relationships and reduce their values of rms, we need to enlarge the sample of SNe observed at these wavelengths. For the J-band, we plot (lower-left panel of Fig. 8) the predictions by Kasen (2006). In the lower-left panel of Fig. 8, we compare the observed quantities for the J-band with the theoretical models provided by Kasen (2006, see their Fig. 11). To reach our goal, we evaluate the ^{56}Ni mass value through the Mazzali et al. (2007) empirical relation. We found a quite good agreement with Kasen (2006) models reproducing the mid-range decliners ($1.1 \lesssim \Delta m_{15}(B) \lesssim 1.3$), whereas, some discrepancy can be noticed in the 'region' of the slow decliners ($\Delta m_{15}(B) \lesssim 1.$) where the secondary maximum occurs later than expected. In contrast, SNe having $\Delta m_{15}(B) \gtrsim 1.4$ show an early appearance of the secondary NIR peak with respect to the model predictions.

By adopting the nomenclature of Kasen (2006), we derived the following parameters from the quantities listed in Table 15: *i*) the difference in magnitude between the secondary maximum and the local minimum, $M_2 - M_0$; and *ii*) the difference in magnitude between the secondary and the primary maximum, $M_2 - M_1$. The results of the comparison between the observations and the models are reported in Fig. 9 as a function of $\Delta m_{15}(B)$. In the *upper panel* of Fig. 9, a close agreement is also found between models and data for what concerns the strengths of the secondary NIR peaks (measured with respect to the local minimum), even though the relatively wide spread of the involved quantities has to be taken into account. Finally, we note that the strengths of the secondary maximum (but now measured with respect to the primary maximum) does not correlate with the decline rate and, the observational data are not closely reproduced by the models (see the *lower panel* of Fig. 9). Our analysis suggest that additional parameters, such as e.g. the outward mixing of ^{56}Ni, could also have strong effects on the secondary maximum, playing a major role in these relations. This confirms the similar conclusions of Kasen (2006, in the discussion of his models), and Folatelli et al. (2010, based on the I-band observations).

As already mentioned, we are still far from achieving a reliable and precise description of all the morphology of NIR light curves of SNe, a goal that will require additional observational and theoretical efforts.

Before concluding, we take further advantage of the entire SNe sample collected here by following the idea suggested by Hamuy et al. (1996a) and Elias-Rosa et al. (2008) for the I-band, i.e. of searching for alternative characterizations of the SN Ia decline rates by comparing $\Delta m_{15}(B)$ with the values of $\Delta m_t(X)$.

The results are shown in Fig. 10. One of these is that a possible linear correlation is found between $\Delta m_{15}(J)$ and the $\Delta m_{15}(B)$. The fit procedure recovers a $R \sim 0.5$ and a scatter of about 0.3 mag, if the SN 2004dt is excluded from the sample on the basis of its spectroscopic and photometric peculiarities (Branch et al. 2009; Biscardi et al., in prep.). In contrast, no correlation is observed between $\Delta m_{15}(H, K)$ and $\Delta m_{15}(B)$.

We also confirm and support the result obtained by Folatelli et al. (2010) for a sample of 9 SNe in the J and H-band: the tightness of the correlation increases when the $\Delta m_{15}(B)$ is compared

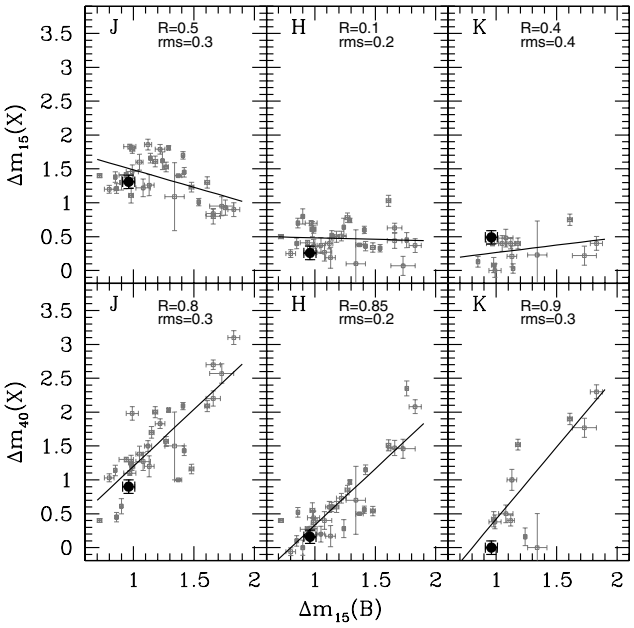

Fig. 10. Comparison of the decline rate Δm_{15} and Δm_{40} in JHK-band (as labeled) versus the $\Delta m_{15}(B)$. The Pearson coefficients R is also shown for each panel with the resulting best fit of data (*solid line*).

to a $\Delta m_{40}(X)$ obtained at later epochs (40 days). This appears evident in the *lower panel* of the same figure: the correlation coefficients range between the 0.8 for the J-band and 0.85 in the H-band. A similar trend is also shown in the K-band, where the sample is limited to only 8 SNe Ia. In this case, we found a correlation coefficient of 0.9, with a scatter of 0.3 mag. This latter conclusion clearly needs to be confirmed, for example by collecting a large number of well-sampled LCs in the K-band.

5. Conclusions

We have presented optical and near-infrared photometric observations of the type Ia SN 2008fv. The observations span a period of about ~65 days. SN 2008fv is a slowly declining SN, for which $\Delta m_{15}(B) = 0.96 \pm 0.08$. The comparison with other available SNe shows that the LC trends, both in the optical rather than in NIR bands, are very similar to SN 2000E.

An estimate of the host galaxy extinction was also obtained by using the optical colour curves and the (V minus NIR) colour curves. A final $E(B-V)_{\rm host} = 0.22 \pm 0.08$ mag is adopted as the most robust evaluation and a value of $R_V = 2.9 \pm 0.2$ is also derived. Assuming these estimates and a Galactic extinction given by Schlegel et al. (1998), we found a mean distance modulus of 33.2 ± 0.1 mag for the host galaxy NGC 3147.

The rise time of SN 2008fv to the B-band maximum was evaluated to be 19.1 ± 0.2 days, slightly shorter (by about a couple of days) than the value typically observed in SN with similar $\Delta m_{15}(B)$ (Riess et al. 1999). Moreover, we derived an ejected ^{56}Ni mass of about $0.7 \pm 0.2\ M_{\odot}$ by analyzing the bolometric light-curve that we obtained here. We note that the quoted evaluation is quite close to the value of ^{56}Ni mass derived by using the empirical relation between $\Delta m_{15}(B)$ and the $M_{\rm Ni}$ (Mazzali et al. 2007).

Finally, we investigated some possible correlations between the optical properties and NIR features of LCs for 40 SNe. As a result, we compiled a set of empirical relations in Eqs. (5)−(7) between the epoch of secondary maximum t_2 and the decline rate $\Delta m_{15}(B)$.

The existence of a strong correlation between the timing of the secondary NIR maximum and the decline rate was confirmed and a quite good agreement with models was found, at least for $1.1 \lesssim \Delta m_{15}(B) \lesssim 1.3$. Moreover, we obtained a correlation between Δm_{40} for J and H band and $\Delta m_{15}(B)$. A similar result in the K-band was uncertain owing to the small number of available LCs for this filter.

We also studied the behaviour of the secondary maxima in the JHK bands with the aim of identify the physical quantities that may play a role in determining the observed morphology of LC in the NIR. Even if the Ni mass observed in the ejecta plays a major role, we agree with other authors (Kasen and Folatelli et al.) that additional quantities (e.g. the outward mixing of ^{56}Ni) have to be taken into account in attempting to understand the features of the SNe LCs in the NIR bands. Nevertheless, the relatively small amount of complete and homogeneous LCs in both the NIR and optical bands have enabled us to state that a focused observational efforts will be required to provide a solid and reliable sample that will permit to probe the models of type Ia SNe.

Acknowledgements. It is a pleasure to acknowledge Prof. A. Tornambè for stimulating discussions. We thank the anonymous referee for detailed reports and constructive criticism that improved this paper. Part of this work was supported by PRIN-INAF 2008 (PI: G. Marconi) and ASI I/016/07.

References

Ajhar, E. A., Tonry, J. L., Blakeslee, J. P., Riess, A. G., & Schmidt, B. P. 2001, ApJ, 559, 584
Altavilla, G., Fiorentino, G., Marconi, M., et al. 2004, MNRAS, 349, 1344
Arnett, W. D. 1982, ApJ, 253, 785
Bessell, M. S. 1979, PASP, 91, 589
Bessell, M. S. 1990, PASP, 102, 1181
Branch, D., Dang, L. C., & Baron, E. 2009, PASP, 121, 238
Brocato, E., & Dolci, M. 2003, Mem. Soc. Astron. It., 74, 110
Buonanno, R., Corsi, C. E., de Biase, G. A., & Ferraro, I. 1979, in Image Processing in Astronomy, ed. G. Sedmak, M. Capaccioli & R. J. Allen, 354
Buonanno, R., Buscema, G., Corsi, C. E., Ferraro, I., & Iannicola, G. 1983, A&A, 126, 278
Candia, P., Krisciunas, K., Suntzeff, N. B., et al. 2003, PASP, 115, 277
Cardelli, J. A., Clayton, G. C., & Mathis, J. S. 1989, ApJ, 345, 245
Challis, P. 2008, Central Bureau Electronic Telegrams, 1522, 1
Contardo, G., Leibundgut, B., & Vacca, W. D. 2000, A&A, 359, 876
Duszanowicz, G. 2006, IAU Circ., 8755, 3
Elias, J. H., Frogel, J. A., Hackwell, J. A., & Persson, S. E. 1981, ApJ, 251, L13
Elias, J. H., Matthews, K., Neugebauer, G., & Persson, S. E. 1985, ApJ, 296, 379
Elias-Rosa, N., Benetti, S., Turatto, M., et al. 2008, MNRAS, 384, 107
Folatelli, G., Phillips, M. M., Burns, C. R., et al. 2010, AJ, 139, 120
Frogel, J. A., Gregory, B., Kawara, K., et al. 1987, ApJ, 315, L129
Ganeshalingam, M., Li, W., & Filippenko, A. V. 2011, MNRAS, 1265
Guy, J., Astier, P., Nobili, S., Regnault, N., & Pain, R. 2005, A&A, 443, 781
Hamuy, M., Phillips, M. M., Wells, L. A., & Maza, J. 1993, PASP, 105, 787
Hamuy, M., Phillips, M. M., Suntzeff, N. B., et al. 1996a, AJ, 112, 2391
Hamuy, M., Phillips, M. M., Suntzeff, N. B., et al. 1996b, AJ, 112, 2438
Hamuy, M., Maza, J., Pinto, P. A., et al. 2002, AJ, 124, 417
Hicken, M., Wood-Vasey, W. M., Blondin, S., et al. 2009, ApJ, 700, 1097
Hoflich, P., Khokhlov, A. M., & Wheeler, J. C. 1995, ApJ, 444, 831
Hsiao, E. Y., Conley, A., Howell, D. A., et al. 2007, ApJ, 663, 1187
Jensen, J. B., Tonry, J. L., Barris, B. J., et al. 2003, ApJ, 583, 712
Jha, S., Kirshner, R. P., Challis, P., et al. 2006, AJ, 131, 527
Johnson, H. L. 1965, ApJ, 141, 923
Kasen, D. 2006, ApJ, 649, 939
Krisciunas, K., Phillips, M. M., Stubbs, C., et al. 2001, AJ, 122, 1616
Krisciunas, K., Suntzeff, N. B., Candia, P., et al. 2003, AJ, 125, 166
Krisciunas, K., Phillips, M. M., & Suntzeff, N. B. 2004a, ApJ, 602, L81
Krisciunas, K., Phillips, M. M., Suntzeff, N. B., et al. 2004b, AJ, 127, 1664
Krisciunas, K., Suntzeff, N. B., Phillips, M. M., et al. 2004c, AJ, 128, 3034
Krisciunas, K., Garnavich, P. M., Stanishev, V., et al. 2007, AJ, 133, 58
Krisciunas, K., Marion, G. H., Suntzeff, N. B., et al. 2009, AJ, 138, 1584
Leibundgut, B. 1990, A&A, 229, 1
Leloudas, G., Stritzinger, M. D., Sollerman, J., et al. 2009, A&A, 505, 265
Li, W., Chornock, R., Leaman, J., et al. 2011, MNRAS, 412, 1473
Lira, P. 1995, Master's Thesis, Univ. Chile

Mannucci, F., Della Valle, M., Panagia, N., et al. 2005, A&A, 433, 807
Mazzali, P. A., Röpke, F. K., Benetti, S., & Hillebrandt, W. 2007, Science, 315, 825
Meikle, W. P. S. 2000, MNRAS, 314, 782
Moffett, T. J., & Barnes, III, T. G. 1979, PASP, 91, 180
Moore, M., & Li, W. 2004, IAU Circ., 8386, 1
Nobili, S., Amanullah, R., Garavini, G., et al. 2005, A&A, 437, 789
Nugent, P., Kim, A., & Perlmutter, S. 2002, PASP, 114, 803
Oja, T. 1996, Baltic Astron., 5, 103
Patat, F., Barbon, R., Cappellaro, E., & Turatto, M. 1997, A&A, 317, 423
Perlmutter, S., Gabi, S., Goldhaber, G., et al. 1997, ApJ, 483, 565
Persson, S. E., Murphy, D. C., Krzeminski, W., Roth, M., & Rieke, M. J. 1998, AJ, 116, 2475
Phillips, M. M. 1993, ApJ, 413, L105
Phillips, M. M., Lira, P., Suntzeff, N. B., et al. 1999, AJ, 118, 1766
Phillips, M. M., Krisciunas, K., Suntzeff, N. B., et al. 2003, in From Twilight to Highlight: The Physics of Supernovae, ed. W. Hillebrandt & B. Leibundgut, 193
Phillips, M. M., Krisciunas, K., Suntzeff, N. B., et al. 2006, AJ, 131, 2615
Pignata, G., Benetti, S., Mazzali, P. A., et al. 2008, MNRAS, 388, 971
Pinto, P. A., & Eastman, R. G. 2000a, ApJ, 530, 744
Pinto, P. A., & Eastman, R. G. 2000b, ApJ, 530, 757
Prieto, J. L., Rest, A., & Suntzeff, N. B. 2006, ApJ, 647, 501
Reindl, B., Tammann, G. A., Sandage, A., & Saha, A. 2005, ApJ, 624, 532
Riess, A. G., Press, W. H., & Kirshner, R. P. 1996, ApJ, 473, 88
Riess, A. G., Filippenko, A. V., Li, W., et al. 1999, AJ, 118, 2675
Saha, A., Thim, F., Tammann, G. A., Reindl, B., & Sandage, A. 2006, ApJS, 165, 108
Schlegel, D. J., Finkbeiner, D. P., & Davis, M. 1998, ApJ, 500, 525
Stritzinger, M., & Leibundgut, B. 2005, A&A, 431, 423
Strolger, L., Smith, R. C., Suntzeff, N. B., et al. 2002, AJ, 124, 2905
Suntzeff, N. B. 1996, in Supernovae and Supernova Remnants, IAU Colloq., 145, 41
Terry, J. N., Paturel, G., & Ekholm, T. 2002, A&A, 393, 57
Thöne, C. C., Michałowski, M. J., Leloudas, G., et al. 2009, ApJ, 698, 1307
Tokunaga, A. T., & Vacca, W. D. 2005, PASP, 117, 421
Tonry, J. L., Dressler, A., Blakeslee, J. P., et al. 2001, ApJ, 546, 681
Tripp, R. 1998, A&A, 331, 815
Tripp, R., & Branch, D. 1999, ApJ, 525, 209
Tully, R. B. 1988, Nearby galaxies catalog, ed. R. B. Tully
Valencic, L. A., Clayton, G. C., & Gordon, K. D. 2004, ApJ, 616, 912
Valentini, G., Di Carlo, E., Massi, F., et al. 2003, ApJ, 595, 779
Wang, L., Goldhaber, G., Aldering, G., & Perlmutter, S. 2003, ApJ, 590, 944
Wang, X., Wang, L., Zhou, X., Lou, Y., & Li, Z. 2005, ApJ, 620, L87
Wang, X., Wang, L., Pain, R., Zhou, X., & Li, Z. 2006, ApJ, 645, 488
Wheeler, J. C., Hoeflich, P., Harkness, R. P., & Spyromilio, J. 1998, ApJ, 496, 908
Willick, J. A., Courteau, S., Faber, S. M., et al. 1997, ApJS, 109, 333
Wood-Vasey, W. M., Friedman, A. S., Bloom, J. S., et al. 2008, ApJ, 689, 377

Pages 13 to 16 are available in the electronic edition of the journal at http://www.aanda.org

Table 6. Transmission curves of BVRI filters.

λ (Å)	B	V	R	I
3400	0.0152	0.0354	0.0491	0.0865
3600	0.0250	0.0517	0.0835	0.1381
3800	0.1036	0.0284	0.0466	0.0818
4000	0.3419	0.0139	0.0220	0.0600
4200	0.6680	0.0081	0.0172	0.0351
4400	0.8546	0.0094	0.0100	0.0204
4500	1.0000	0.0102	0.0107	0.0219
4600	0.9728	0.0108	0.0114	0.0232
4800	0.6620	0.1960	0.0123	0.0249
5000	0.2962	0.8784	0.0127	0.0260
5200	0.0000	0.9787	0.0131	0.0133
5300	0.0000	1.0000	0.0132	0.0135
5400	0.0000	0.9921	0.0133	0.0136
5700	0.0000	0.8396	0.5818	0.0135
5900	0.0000	0.6609	0.9999	0.0000
6000	0.0000	0.5487	1.000	0.0137
6100	0.0000	0.4493	0.9612	0.0135
6500	0.0000	0.1226	0.7500	0.0000
7000	0.0000	0.0118	0.4263	0.0128
7500	0.0000	0.0000	0.1702	0.9995
7600	0.0000	0.0000	0.1317	1.0000
7700	0.0000	0.0000	0.0965	0.9992
7800	0.0000	0.0000	0.0707	0.9419
7900	0.0000	0.0000	0.0612	0.9506
8000	0.0000	0.0000	0.0391	0.9114
8200	0.0000	0.0000	0.0183	0.8453
8500	0.0000	0.0000	0.0074	0.6768
9000	0.0000	0.0000	0.0000	0.4450
9500	0.0000	0.0000	0.0000	0.2771
1.00e+04	0.0000	0.0000	0.0000	0.0580
1.05e+04	0.0000	0.0000	0.0000	0.0000

Table 7. Transmission curves of BVRI filters.

λ (Å)	J	λ (Å)	H	λ (Å)	K
1.08e+04	0.0203	1.49e+04	0.0150	1.97e+04	0.0233
1.1e+04	0.1449	1.50e+04	0.0530	1.98e+04	0.0620
1.12e+04	0.1981	1.51e+04	0.1570	1.99e+04	0.1391
1.13e+04	0.2589	1.52e+04	0.3295	2.00e+04	0.2315
1.14e+04	0.2395	1.53e+04	0.5002	2.01e+04	0.2382
1.15e+04	0.3046	1.54e+04	0.5634	2.02e+04	0.3763
1.16e+04	0.3400	1.55e+04	0.6506	2.03e+04	0.5431
1.17e+04	0.4952	1.56e+04	0.6972	2.04e+04	0.6956
1.18e+04	0.5652	1.57e+04	0.7096	2.05e+04	0.5952
1.19e+04	0.6738	1.58e+04	0.7205	2.06e+04	0.6523
1.20e+04	0.6913	1.59e+04	0.8070	2.07e+04	0.6575
1.21e+04	0.7457	1.60e+04	0.8018	2.08e+04	0.7917
1.22e+04	0.7952	1.61e+04	0.8043	2.09e+04	0.8668
1.23e+04	0.8186	1.62e+04	0.8094	2.10e+04	0.8638
1.24e+04	0.8378	1.63e+04	0.8517	2.11e+04	0.8461
1.25e+04	0.8679	1.64e+04	0.8989	2.12e+04	0.8614
1.26e+04	0.8317	1.65e+04	0.898	2.13e+04	0.8883
1.27e+04	0.7962	1.66e+04	0.9011	2.14e+04	0.9049
1.28e+04	0.9360	1.67e+04	0.9246	2.15e+04	0.9453
1.29e+04	0.9872	1.68e+04	0.9250	2.16e+04	0.9337
1.30e+04	0.9722	1.69e+04	0.947	2.17e+04	0.9364
1.31e+04	0.9533	1.70e+04	0.907	2.18e+04	0.9718
1.32e+04	0.9143	1.71e+04	0.9460	2.19e+04	0.9420
1.33e+04	0.7560	1.72e+04	0.9472	2.20e+04	0.9994
1.34e+04	0.6024	1.73e+04	0.9726	2.21e+04	0.9928
1.35e+04	0.5233	1.74e+04	0.9760	2.22e+04	0.9763
1.36e+04	0.4749	1.75e+04	0.9518	2.23e+04	0.9774
1.37e+04	0.4620	1.76e+04	0.9524	2.24e+04	0.9278
1.38e+04	0.4370	1.77e+04	0.9585	2.25e+04	0.8814
1.39e+04	0.3225	1.78e+04	0.8456	2.26e+04	0.8463
1.40e+04	0.2483	1.79e+04	0.6995	2.27e+04	0.7852
1.42e+04	0.0532	1.80e+04	0.4263	2.271e+04	0.7741
1.43e+04	0.0193	1.81e+04	0.2120	2.28e+04	0.7110
1.44e+04	0.0079	1.82e+04	0.0382	2.29e+04	0.7070
1.45e+04	0.0000	1.83e+04	0.0152	2.30e+04	0.7246
1.46e+04	0.0000	1.84e+04	0.0022	2.31e+04	0.6041
1.47e+04	0.0000	1.85e+04	0.0022	2.32e+04	0.4858
1.48e+04	0.0000	1.86e+04	0.0014	2.33e+04	0.3610
		1.87e+04	0.0000	2.34e+04	0.1972
				2.35e+04	0.1091
				2.36e+04	0.0594
				2.37e+04	0.0342
				2.38e+04	0.0226
				2.39e+04	0.0138
				2.40e+04	0.0049
				2.41e+04	0.0000

Table 15. Light curves parameters for our selected sample of SNe Ia.

SN (1)	$\Delta m_{15}(B)$ (2)	$T(B_{\max})$ (3)	A_X (4)	m_1 (5)	$T(X_2)$ (6)	m_2 (7)	m_0 (8)	$\Delta m_{15}(X)$ (9)	$\Delta m_{40}(X)$ (10)	μ (11)	$M_{1,X}$ (12)	$t_{2,X}$ (13)	$M_{2,X}$ (14)	$M_{0,X}$ (15)
							J-band							
SN1986g[1]	1.73 ± 0.1	561.5 ± 1.0	0.82	–	578.0 ± 0.5	10.99 ± 0.1	11.03 ± 0.1	0.95 ± 0.1	2.57 ± 0.1	27.8 ± 0.1[a]	–	16.5 ± 1.4	−16.8 ± 0.1	−16.8 ± 0.1
SN1999ac[2]	1.34 ± 0.08	1251.0 ± 0.5	0.15	14.51 ± 0.04	1278.0 ± 2.0	15.61 ± 0.5	15.76 ± 0.02	1.09 ± 0.5	1.5 ± 0.5	33.5 ± 0.3[b]	−18.99 ± 0.3	27.0 ± 2.	−17.9 ± 0.3	−17.7 ± 0.3
SN1999ee[3]	0.94 ± 0.06	1469.1 ± 0.5	0.29	14.82 ± 0.02	1503.5 ± 0.5	15.89 ± 0.03	16.43 ± 0.02	1.41 ± 0.04	1.3 ± 0.04	33.2 ± 0.2[b]	−18.38 ± 0.2	34.4 ± 0.7	−17.3 ± 0.2	−16.8 ± 0.2
SN1999ek[4]	1.17 ± 0.03	1481.8 ± 0.1	0.68	16.10 ± 0.07	–	–	17.82 ± 0.08	–	–	34.4 ± 0.3[d]	−18.3 ± 0.3	–	–	−15.6 ± 0.3
SN2000E[5]	0.99 ± 0.05	1577.0 ± 0.5	0.43	13.48 ± 0.01	1608.8 ± 0.5	14.46 ± 0.1	14.94 ± 0.03	1.46 ± 0.1	2.0 ± 0.1	31.9 ± 0.4[c]	−18.42 ± 0.4	31.85 ± 0.7	−17.4 ± 0.4	−17.0 ± 0.4
SN2000bh[3]	1.16 ± 0.1	1635.2 ± 0.3	0.06	–	1668.5 ± 0.5	17.33 ± 0.03	18.37 ± 0.04	–	–	34.6 ± 0.3*	–	33.3 ± 0.6	−17.3 ± 0.3	−16.2 ± 0.3
SN2000bk[6]	1.63 ± 0.1	1647.9 ± 0.2	0.06	–	1671.9 ± 0.5	18.03 ± 0.05	18.66 ± 0.05	–	–	35.8 ± 0.2*	–	24 ± 0.5	−17.7 ± 0.2	−17.1 ± 0.2
SN2001ba[3]	0.97 ± 0.05	2034.5 ± 0.7	0.08	16.99 ± 0.02	2068.5 ± 0.5	18.01 ± 0.03	18.87 ± 0.08	1.83 ± 0.03	1.1 ± 0.04	35.4 ± 0.2[b]	−18.41 ± 0.2	34.0 ± 0.9	−17.4 ± 0.2	−16.5 ± 0.2
SN2001bt[4]	1.18 ± 0.02	2063.4 ± 0.2	0.29	15.34 ± 0.07	2091.7 ± 0.5	16.43 ± 0.04	17.17 ± 0.07	1.61 ± 0.08	2.0 ± 0.08	34.1 ± 0.4[a]	−18.8 ± 0.4	28.3 ± 0.5	−17.7 ± 0.4	−16.9 ± 0.4
SN2001cn[4]	1.15 ± 0.02	2071.6 ± 0.2	0.19	15.61 ± 0.08	2101.7 ± 0.5	16.56 ± 0.03	17.19 ± 0.04	–	1.7 ± 0.08	34.1 ± 0.2*	−18.49 ± 0.2	30.1 ± 0.5	−17.5 ± 0.2	−16.9 ± 0.2
SN2001cz[4]	1.05 ± 0.03	2103.9 ± 0.1	0.19	15.49 ± 0.06	2137.5 ± 0.5	16.69 ± 0.1	17.4 ± 0.12	1.60 ± 0.1	1.38 ± 0.1	33.5 ± 0.1[a]	−18.01 ± 0.2	34.0 ± 0.5	−16.8 ± 0.1	−16. ± 0.1
SN2001el[7]	1.13 ± 0.04	2182.5 ± 0.5	0.19	12.90 ± 0.04	2213.7 ± 0.5	13.92 ± 0.15	14.30 ± 0.04	1.26 ± 0.1	1.2 ± 0.1	31.3 ± 0.4[a]	−18.4 ± 0.4	31.2 ± 0.7	−17.4 ± 0.4	−17.0 ± 0.4
SN2002bo[4]	1.12 ± 0.03	2356.5 ± 0.2	0.34	13.62 ± 0.07	2385.6 ± 0.5	14.76 ± 0.04	15.57 ± 0.05	1.86 ± 0.08	1.5 ± 0.08	31.8 ± 0.8[c]	−18.18 ± 0.8	29.1 ± 0.5	−17.0 ± 0.1	−16.2 ± 0.8
SN2002dj[8]	1.08 ± 0.06	2450.0 ± 0.7	0.03	14.58 ± 0.1	2481.0 ± 0.5	15.50 ± 0.07	16.30 ± 0.09	1.22 ± 0.1	1.27 ± 0.1	32.9 ± 0.2[b]	−18.32 ± 0.2	31 ± 0.9	−17.4 ± 0.2	−16.6 ± 0.2
SN2003gs[9]	1.83 ± 0.05	2848.5 ± 0.5	0.05	13.2 ± 0.1	2863.8 ± 0.5	14.07 ± 0.02	15.96 ± 0.07	0.90 ± 0.1	3.1 ± 0.1	31.7 ± 0.3[a]	−18.5 ± 0.3	15.3 ± 0.7	−17.7 ± 0.3	−15.7 ± 0.3
SN2003hv[10]	1.61 ± 0.02	2891.2 ± 0.3	0.49	12.85 ± 0.08	3114.2 ± 0.5	14.00 ± 0.02	14.19 ± 0.03	1.30 ± 0.08	2.09 ± 0.08	31.4 ± 0.3[e]	−18.55 ± 0.3	23 ± 0.6	−17.4 ± 0.3	−17.2 ± 0.3
SN2004dt[11]	1.20 ± 0.05	3240.5 ± 0.5	0.18	15.72 ± 0.06	3269.0 ± 0.5	16.27 ± 0.06	16.37 ± 0.08	0.36 ± 0.08	0.9 ± 0.08	34.5 ± 0.15*	−18.58 ± 0.2	28.5 ± 0.7	−18.0 ± 0.15	−17.9 ± 0.2
SN2004ey[12]	0.98 ± 0.02	3301.5 ± 0.5	0.13	15.5 ± 0.1	3337.0 ± 0.5	16.60 ± 0.05	16.99 ± 0.05	1.11 ± 0.1	1.25 ± 0.1	34.1 ± 0.1*	−18.6 ± 0.2	35.5 ± 0.7	−17.5 ± 0.1	−17.1 ± 0.1
SN2004eo[12]	1.37 ± 0.03	3279.5 ± 0.5	0.07	15.51 ± 0.01	3303.5 ± 0.5	16.69 ± 0.01	17.14 ± 0.1	1.42 ± 0.01	1.00 ± 0.02	34.2 ± 0.15*	−18.69 ± 0.1	24 ± 0.7	−17.5 ± 0.15	−17.0 ± 0.1
SN2004gs[12]	1.54 ± 0.01	3357.5 ± 0.5	0.11	17.27 ± 0.05	3379.0 ± 0.5	18.1 ± 0.02	18.31 ± 0.02	1.01 ± 0.05	–	35.3 ± 0.1*	−18.03 ± 0.3	21.5 ± 0.7	−17.2 ± 0.15	−17.0 ± 0.1
SN2004gu[12]	0.80 ± 0.04	3360.0 ± 0.5	0.22	17.79 ± 0.03	3394.0 ± 0 3	18.80 ± 0.05	19.29 ± 0.07	1.20 ± 0.05	1.03 ± 0.06	36.4 ± 0.1*	−18.61 ± 0.1	34 ± 3	−17.6 ± 0.1	−17.1 ± 0.1
SN2005A[12]	1.17 ± 0.03	3380.0 ± 0.5	0.93	16.88 ± 0.03	3407.6 ± 0.5	17.97 ± 0.05	18.16 ± 0.02	1.48 ± 0.05	1.19 ± 0.06	34.5 ± 0.06*	−17.58 ± 0.07	27.6 ± 0.7	−16.5 ± 0.09	−16.3 ± 0.06
SN2005M[12]	0.85 ± 0.01	3406.0 ± 0.5	0.09	16.48 ± 0.06	3437.0 ± 0.5	17.55 ± 0.05	18.04 ± 0.02	1.38 ± 0.07	1.14 ± 0.08	35.1 ± 0.1*	−18.62 ± 0.4	31 ± 0.7	−17.5 ± 0.1	−17.0 ± 0.1
SN2005ag[12]	0.86 ± 0.01	3416.8 ± 1.0	0.29	19.19 ± 0.0	3451.8 ± 0.5	19.62 ± 0.0	20.55 ± 0.05	1.21 ± 0.07	0.44 ± 0.07	37.5 ± 0.1*	−18.31 ± 0.1	35 ± 1.1	−18.0 ± 0.1	−16.9 ± 0.1
SN2005al[12]	1.22 ± 0.04	3430.0 ± 0.5	0.27	15.46 ± 0.05	3454.9 ± 0.5	16.70 ± 0.05	17.25 ± 0.05	1.79 ± 0.07	1.83 ± 0.07	34.1 ± 0.1*	−18.64 ± 0.1	24.9 ± 0.7	−17.4 ± 0.1	−16.8 ± 0.1
SN2005am[12]	1.48 ± 0.02	3436.1 ± 0.5	0.00	14.04 ± 0.05	3456.5 ± 0.5	15.16 ± 0.05	15.30 ± 0.05	1.23 ± 0.07	1.16 ± 0.07	33.6 ± 0.2*	−19.56 ± 0.2	20.4 ± 0.7	−18.4 ± 0.21	−18.3 ± 0.2
SN2005el[12]	1.29 ± 0.01	3645. ± 0.5	0.05	15.47 ± 0.01	3672.0 ± 0.5	16.62 ± 0.03	17.36 ± 0.06	1.81 ± 0.03	2.03 ± 0.03	33.9 ± 0.15*	−18.43 ± 0.4	27 ± 0.7	−17.3 ± 0.15	−16.5 ± 0.1
SN2005eq[12]	0.72 ± 0.02	3655.5 ± 0.5	0.16	16.79 ± 0.02	3690.5 ± 0.5	17.79 ± 0.02	18.35 ± 0.1	1.40 ± 0.02	0.4 ± 0.02	35.3 ± 0.15*	−18.51 ± 0.1	35 ± 0.7	−17.5 ± 0.15	−16.9 ± 0.1
SN2005hc[12]	0.90 ± 0.01	3668.7 ± 0.5	0.08	17.93 ± 0.05	3703.0 ± 2.0	18.49 ± 0.1	18.94 ± 0.05	1.30 ± 0.1	0.61 ± 0.1	36.5 ± 0.05*	−18.57 ± 0.8	34.3 ± 2.0	−18.0 ± 0.1	−17.6 ± 0.07
SN2005iq[12]	1.24 ± 0.01	3687.5 ± 0.5	0.01	17.28 ± 0.02	3715.5 ± 0.5	18.69 ± 0.13	18.94 ± 0.2	1.62 ± 0.1	0.28 ± 0.1	32.9 ± 0.15*	−15.62 ± 0.1	28 ± 0.7	−14.2 ± 0.1	−14.0 ± 0.2
SN2005ke[12]	1.76 ± 0.01	3700.7 ± 0.5	0.06	14.00 ± 0.05	3721.0 ± 0.5	15.05 ± 0.1	14.64 ± 0.1	0.93 ± 0.1	3.55 ± 0.1	31.4 ± 0.15*	−17.4 ± 0.2	–	−16.35 ± 0.2	−16.76 ± 0.2
SN2005ki[12]	1.27 ± 0.02	3706.8 ± 0.5	0.09	16.22 ± 0.05	3732.8 ± 0.5	17.37 ± 0.05	17.83 ± 0.04	1.53 ± 0.07	1.57 ± 0.07	34.6 ± 0.04*	−18.38 ± 0.1	26 ± 0.7	−17.20 ± 0.06	−16.8 ± 0.06
SN2005kc[12]	1.14 ± 0.01	3698.6 ± 0.5	0.08	15.49 ± 0.06	3727.4 ± 0.5	16.58 ± 0.05	17.15 ± 0.05	1.66 ± 0.07	1.61 ± 0.08	33.9 ± 0.05*	−18.45 ± 0.07	28.8 ± 0.7	−17.5 ± 0.07	−16.8 ± 0.07
SN2006D[12]	1.42 ± 0.01	3758.8 ± 0.5	0.02	14.40 ± 0.05	3782.9 ± 0.5	15.64 ± 0.05	16.03 ± 0.05	1.45 ± 0.07	1.43 ± 0.07	32.9 ± 0.15*	−18.5 ± 0.1	24.1 ± 0.7	−17.3 ± 0.15	−17.0 ± 0.1
SN2006X[12]	1.09 ± 0.01	3786.8 ± 0.5	1.13	13.64 ± 0.01	3813.8 ± 0.5	14.58 ± 0.01	15.34 ± 0.01	1.65 ± 0.01	1.35 ± 0.02	31.2 ± 0.05[f]	−17.4 ± 0.07	27 ± 0.7	−16.5 ± 0.07	−15.7 ± 0.07
SN2006ax[12]	0.99 ± 0.02	3828.5 ± 0.5	0.00	15.69 ± 0.03	3860.0 ± 0.5	16.89 ± 0.05	17.33 ± 0.03	1.79 ± 0.05	1.2 ± 0.06	34.3 ± 0.05*	−18.61 ± 0.1	31.5 ± 0.7	−17.4 ± 0.06	−17.0 ± 0.05
SN2006bh[12]	1.41 ± 0.01	3833.9 ± 0.5	0.15	14.80 ± 0.02	3857.0 ± 0.5	16.09 ± 0.05	16.56 ± 0.06	1.7 ± 0.05	2.09 ± 0.05	33.3 ± 0.1*	−18.5 ± 0.07	23.1 ± 0.7	−17.2 ± 0.1	−16.7 ± 0.1
SN2006eq[12]	1.66 ± 0.06	3976.0 ± 0.5	0.19	18.36 ± 0.05	3999.5 ± 0.5	19.06 ± 0.1	19.1 ± 0.05	0.8 ± 0.1	2.2 ± 0.1	36.5 ± 0.1*	−18.14 ± 0.1	23.5 ± 0.7	−17.4 ± 0.1	−17.4 ± 0.1
SN2006gt[12]	1.66 ± 0.06	4002.7 ± 0.5	0.16	18.14 ± 0.05	4029.6 ± 0.5	19.40 ± 0.05	19.08 ± 0.05	0.84 ± 0.07	2.7 ± 0.07	36.5 ± 0.1*	−18.36 ± 0.1	26.9 ± 0.7	−17.1 ± 0.1	−17.4 ± 0.1
SN2008fv[13]	0.96 ± 0.05	4749.8 ± 0.2	0.17	14.60 ± 0.07	4780.1 ± 0.5	15.48 ± 0.07	16.06 ± 0.05	1.3 ± 0.1	0.9 ± 0.1	33.1 ± 0.8[c]	−18.5 ± 0.8	30.3 ± 0.5	−17.6 ± 0.8	−17.0 ± 0.8
							H-band							
SN1986g	1.73 ± 0.1	561.5 ± 1.0	0.59	9.93 ± 0.1	574.0 ± 1	10.0 ± 0.1	9.62 ± 0.1	0.07 ± 0.1	1.46 ± 0.1	27.8 ± 0.1	−17.88 ± 0.1	12.5 ± 1.4	−17.8 ± 0.1	–
SN1999ac	1.34 ± 0.08	1251.0 ± 0.5	0.10	14.67 ± 0.04	–	–	14.84 ± 0.02	0.10 ± 0.5	0.70 ± 0.5	33.5 ± 0.3	−18.83 ± 0.3	–	–	−18.7 ± 0.3
SN1999ee	0.94 ± 0.06	1469.1 ± 0.5	0.21	14.93 ± 0.03	1499.6 ± 0.5	15.11 ± 0.03	15.52 ± 0.04	0.41 ± 0.04	0.27 ± 0.04	33.2 ± 0.2	−18.27 ± 0.2	30.5 ± 0.7	−18.1 ± 0.2	−17.7 ± 0.3
SN1999ek	1.17 ± 0.03	1481.8 ± 0.11	0.46	16.30 ± 0.08	–	–	16.48 ± 0.02	0.18 ± 0.08	–	34.4 ± 0.3	−18.1 ± 0.3	–	–	16.48 ± 0.02
SN2000E	0.99 ± 0.05	1577.0 ± 0.5	0.34	13.76 ± 0.07	1602.1 ± 0.5	13.85 ± 0.1	14.13 ± 0.08	0.4 ± 0.1	0.4 ± 0.1	31.9 ± 0.4	−18.15 ± 0.4	25.1 ± 0.7	−18.0 ± 0.4	−17.8 ± 0.4
SN2000bh	1.16 ± 0.1	1635.2 ± 0.28	0.04	–	1665.5 ± 0.5	16.85 ± 0.04	17.24 ± 0.03	–	–	34.6 ± 0.3	–	30.3 ± 0.6	−17.7 ± 0.3	−17.4 ± 0.3
SN2000bk	1.63 ± 0.1	1647.9 ± 0.2	0.3	–	667.6 ± 0.5	17.45 ± 0.05	–	–	–	35.78 ± 0.2	–	19.7 ± 0.5	−18.3 ± 0.2	–
SN2001ba	0.97 ± 0.05	2034.5 ± 0.7	0.05	17.24 ± 0.03	2057.5 ± 0.5	17.44 ± 0.05	17.94 ± 0.07	0.70 ± 0.04	0.28 ± 0.04	35.4 ± 0.2	−18.16 ± 0.2	23 ± 0.9	−18.0 ± 0.2	−17.3 ± 0.4

Table 15. continued.

SN	$\Delta m_{15}(B)$	$T(B_{\max})$	A_X	m_1	$T(X_2)$	m_2	m_0	$\Delta m_{15}(X)$	$\Delta m_{40}(X)$	μ	$M_{1,X}$	$t_{2,X}$	$M_{2,X}$	$M_{0,X}$
(1)	(2)	(3)	(4)	(5)	(6)	(7)	(8)	(9)	(10)	(11)	(12)	(13)	(14)	(15)
SN2001bt	1.18 ± 0.02	2063.4 ± 0.22	0.20	15.69 ± 0.04	2088.7 ± 0.5	16.65 ± 0.05	16.2 ± 0.2	0.5 ± 0.08	0.6 ± 0.08	34.1 ± 0.4	–18.41 ± 0.4	25.3 ± 0.5	–17.4 ± 0.4	–17.9 ± 0.4
SN2001cn	1.15 ± 0.02	2071.6 ± 0.15	0.14	15.90 ± 0.12	2091.6 ± 0.5	15.83 ± 0.1	16.16 ± 0.06	–	–	34.1 ± 0.2	–18.2 ± 0.2	20 ± 0.5	–18.3 ± 0.2	–17.9 ± 0.2
SN2001cz	1.05 ± 0.03	2103.9 ± 0.12	0.13	15.78 ± 0.12	2132.5 ± 0.5	15.65 ± 0.2	16.1 ± 0.2	0.37 ± 0.08	0.2 ± 0.1	33.5 ± 0.1	–17.72 ± 0.1	28.6 ± 0.5	–17.8 ± 0.1	–17.35 ± 0.25
SN2001el	1.13 ± 0.04	2182.5 ± 0.5	0.13	13.08 ± 0.04	2207.8 ± 0.5	12.97 ± 0.04	13.28 ± 0.04	0.19 ± 0.1	0.18 ± 0.1	31.3 ± 0.4	–18.22 ± 0.4	25.3 ± 0.7	–18.3 ± 0.4	–18.0 ± 0.4
SN2002bo	1.12 ± 0.03	2356.5 ± 0.2	0.24	13.94 ± 0.03	2381.6 ± 0.5	13.89 ± 0.03	14.38 ± 0.05	0.40 ± 0.08	0.60 ± 0.08	31.8 ± 0.8	–17.86 ± 0.8	25.1 ± 0.5	–17.9 ± 0.8	–17.4 ± 0.8
SN2002dj	1.08 ± 0.06	2450.0 ± 0.7	0.20	14.80 ± 0.07	2473.0 ± 0.5	14.75 ± 0.03	–	0.3 ± 0.1	0.40 ± 0.1	32.9 ± 0.2	–18.1 ± 0.2	23 ± 0.9	–18.1 ± 0.2	–
SN2003gs	1.83 ± 0.05	2848.5 ± 0.5	0.03	13.17 ± 0.08	–	–	13.47 ± 0.01	0.37 ± 0.08	2.08 ± 0.09	31.7 ± 0.3	–18.53 ± 0.3	–	–	–18.2 ± 0.2
SN2003hv	1.61 ± 0.02	2891.2 ± 0.3	0.02	13.20 ± 0.08	3110.3 ± 0.5	13.11 ± 0.02	13.50 ± 0.03	1.03 ± 0.08	1.51 ± 0.08	31.4 ± 0.3	–18.2 ± 0.3	19.1 ± 0.6	–18.3 ± 0.3	–17.9 ± 0.3
SN2004dt	1.20 ± 0.05	3240.5 ± 0.5	0.13	15.90 ± 0.07	3262.0 ± 0.5	15.43 ± 0.1		0.22 ± 0.08	0.10 ± 0.08	34.3 ± 0.15	–18.4 ± 0.2	21.5 ± 0.7	–18.9 ± 0.1	–
SN2004gs	1.54 ± 0.01	3357.5 ± 0.5	0.08	17.37 ± 0.05	3376.0 ± 0.5	17.53 ± 0.05	17.81 ± 0.03	0.33 ± 0.05	–	35.3 ± 0.1	–17.93 ± 0.1	18.5 ± 0.7	–17.8 ± 0.1	–17.5 ± 0.1
SN2004gu	0.80 ± 0.04	3360.0 ± 0.5	0.16	18.47 ± 0.1	–	–	–	0.25 ± 0.06	0.10 ± 0.05	36.4 ± 0.1	–17.93 ± 0.1	–	–	–
SN2004ey	0.98 ± 0.02	3301.5 ± 0.5	0.09	15.65 ± 0.08	3332.0 ± 0.5	15.87 ± 0.08	16.16 ± 0.01	0.6 ± 0.1	0.55 ± 0.1	34.1 ± 0.1	–18.45 ± 0.2	30.5 ± 0.7	–18.2 ± 0.1	–17.9 ± 0.1
SN2004eo	1.37 ± 0.03	3279.5 ± 0.5	0.10	15.80 ± 0.03	3301.5 ± 0.5	15.90 ± 0.01	16.14 ± 0.10	0.38 ± 0.02	0.5 ± 0.01	34.2 ± 0.15	–18.4 ± 0.1	22 ± 0.7	–18.3 ± 0.15	16.14 ± 0.1
SN2005A	1.17 ± 0.03	3380.0 ± 0.5	0.04	16.47 ± 0.05	3405.0 ± 0.5	16.51 ± 0.05	16.89 ± 0.02	0.42 ± 0.05	0.33 ± 0.06	34.4 ± 0.06	–17.99 ± 0.07	25 ± 0.7	–18.0 ± 0.1	–17.51 ± 0.06
SN2005M	0.85 ± 0.01	3406.0 ± 0.5	0.06	16.69 ± 0.05	3430.0 ± 0.5	16.55 ± 0.05	17.13 ± 0.02	0.4 ± 0.07	0.1 ± 0.08	35.1 ± 0.1	–18.41 ± 0.1	24 ± 0.7	–18.5 ± 0.1	–18.0 ± 0.1
SN2005al	1.22 ± 0.04	3430.0 ± 0.5	0.00	15.87 ± 0.05	3457.0 ± 0.5	16.00 ± 0.05	16.37 ± 0.05	0.51 ± 0.07	0.73 ± 0.07	34.1 ± 0.1	–18.23 ± 0.1	27 ± 0.7	–18.1 ± 0.1	–18.73 ± 0.15
SN2005am	1.48 ± 0.02	3436.1 ± 0.5	0.04	14.14 ± 0.05	3455.6 ± 0.5	14.46 ± 0.05	–	0.34 ± 0.07	0.54 ± 0.07	33.6 ± 0.2	–19.46 ± 0.2	19.5 ± 0.7	–19.1 ± 0.1	–
SN2005ag	0.86 ± 0.01	3416.8 ± 1.0	0.05	19.02 ± 0.05	3444.0 ± 0.5	19.44 ± 0.05	20.12 ± 0.2	0.7 ± 0.07	0.52 ± 0.07	37.5 ± 0.1	–18.48 ± 0.1	27.2 ± 1.	–18.1 ± 0.1	–17.4 ± 0.2
SN2005el	1.29 ± 0.01	3645. ± 0.5	0.03	15.61 ± 0.02	3671.0 ± 0.5	15.87 ± 0.05	16.36 ± 0.03	0.74 ± 0.03	0.97 ± 0.03	33.9 ± 0.15	–18.29 ± 0.1	26 ± 0.7	–18.0 ± 0.15	–17.5 ± 0.2
SN2005eq	0.72 ± 0.02	3655.5 ± 0.5	0.11	16.91 ± 0.02	3680. ± 1	17.26 ± 0.05	17.71 ± 0.07	0.5 ± 0.03	0.4 ± 0.03	35.3 ± 0.15	–18.39 ± 0.1	24.5 ± 1.1	–18.0 ± 0.15	–17.6 ± 0.2
SN2005hc	0.90 ± 0.01	3668.7 ± 0.5	0.05	17.57 ± 0.05	3696.7 ± 0.5	18.06 ± 0.14	18.55 ± 0.26	0.8 ± 0.1	0.0 ± 0.1	36.5 ± 0.05	–18.93 ± 0.07	28 ± 0.7	–18.4 ± 0.15	17.9 ± 0.3
SN2005iq	1.24 ± 0.01	3687.5 ± 0.5	0.01	17.36 ± 0.05	3710.6 ± 0.5	17.90 ± 0.10	17.96 ± 0.16	0.64 ± 0.1	0.94 ± 0.1	32.9 ± 0.15	–15.54 ± 0.1	23.1 ± 0.7	–15.0 ± 0.15	–14.9 ± 0.2
SN2005ki	1.27 ± 0.02	3706.8 ± 0.5	0.00	16.2 ± 0.05	3728.0 ± 0.5	16.54 ± 0.05	17.02 ± 0.05	0.78 ± 0.07	0.85 ± 0.07	34.6 ± 0.04	–18.4 ± 0.06	21.2 ± 0.7	–18.1 ± 0.2	–17.58 ± 0.06
SN2005kc	1.14 ± 0.01	3698.6 ± 0.5	0.19	15.66 ± 0.05	3721.0 ± 0.5	15.82 ± 0.05	16.10 ± 0.03	0.52 ± 0.07	0.68 ± 0.07	33.9 ± 0.05	–18.28 ± 0.07	22.4 ± 0.7	–18.1 ± 0.07	–17.8 ± 0.05
SN2005ke	1.76 ± 0.01	3700.7 ± 0.5	0.04	13.94 ± 0.07	–	–	17.73 ± 0.05	0.5 ± 0.1	2.3 ± 0.1	31.4 ± 0.15	–17.46 ± 0.2	–	–	–13.67 ± 0.15
SN2006D	1.42 ± 0.01	3758.8 ± 0.5	0.06	14.53 ± 0.05	3779.9 ± 0.5	14.89 ± 0.02	15.00 ± 0.10	0.36 ± 0.07	1.15 ± 0.07	32.9 ± 0.15	–18.37 ± 0.1	21.1 ± 0.7	–18.0 ± 0.15	–17.9 ± 0.2
SN2006X	1.09 ± 0.01	3786.8 ± 0.5	0.82	12.85 ± 0.05	3810.8 ± 0.5	12.97 ± 0.01	13.41 ± 0.01	0.43 ± 0.01	0.47 ± 0.01	31.0 ± 0.07	–18.19 ± 0.09	24 ± 0.7	–18.1 ± 0.1	–17.59 ± 0.07
SN2006ax	0.99 ± 0.02	3828.5 ± 0.5	0.01	15.86 ± 0.05	3855.0 ± 0.5	16.04 ± 0.02	16.51 ± 0.02	0.61 ± 0.05	0.37 ± 0.06	34.3 ± 0.05	–18.44 ± 0.07	26.5 ± 0.7	–18.3 ± 0.06	–17.79 ± 0.05
SN2006bh	1.41 ± 0.01	3833.9 ± 0.5	0.00	14.97 ± 0.01	3855.5 ± 0.5	15.27 ± 0.05	15.61 ± 0.01	0.6 ± 0.05	0.56 ± 0.05	33.3 ± 0.1	–18.33 ± 0.1	21.6 ± 0.7	–18.0 ± 0.1	–17.7 ± 0.1
SN2006eq	1.66 ± 0.06	3976.0 ± 0.5	0.14	18.34 ± 0.05	3995.8 ± 0.5	19.05 ± 0.05	18.63 ± 0.25	0.44 ± 0.1	1.47 ± 0.1	36.5 ± 0.1	–18.16 ± 0.1	19.8 ± 0.7	–17.4 ± 0.1	–17.9 ± 0.3
SN2006gt	1.66 ± 0.06	4002.7 ± 0.5	0.11	18.22 ± 0.05	4020.9 ± 0.5	18.85 ± 0.05	18.62 ± 0.06	0.63 ± 0.1	–	36.5 ± 0.1	–18.28 ± 0.1	18.2 ± 0.7	–17.6 ± 0.1	17.9 ± 0.1
SN2008fv	0.96 ± 0.05	4749.8 ± 0.2	0.11	15.16 ± 0.08	4780.1 ± 0.5	14.99 ± 0.06	15.42 ± 0.05	0.26 ± 0.09	0.16 ± 0.09	33.1 ± 0.8	–17.94 ± 0.8	30.3 ± 0.5	–18.1 ± 0.8	–17.7 ± 0.8
							K-band							
SN1986g	1.73 ± 0.1	561.5 ± 1.0	0.37	10.00 ± 0.1	577.0 ± 1.0	9.97 ± 0.1	9.14 ± 0.1	0.22 ± 0.1	1.77 ± 0.1	27.8 ± 0.1	–19.03 ± 0.1	15.5 ± 1.	–17.8 ± 0.15	–
SN1999ac	1.34 ± 0.08	1251.0 ± 0.5	0.06	–	–	–	14.81 ± 0.02	0.23 ± 0.5	0.97 ± 0.5	33.5 ± 0.3	–	–	–	–18.7 ± 0.3
SN1999ee	0.94 ± 0.06	1469.1 ± 0.5	0.13	15.11 ± 0.03	–	–	–	–	–	33.2 ± 0.2	–18.63 ± 0.2	–	–	–
SN1999ek	1.17 ± 0.03	1481.8 ± 0.11	0.27	–	–	–	–	–	–	34.4 ± 0.3	–	–	–	–
SN2000E	0.99 ± 0.05	1577.0 ± 0.5	0.20	13.85 ± 0.1	1606.1 ± 0.5	13.56 ± 0.1	14.06 ± 0.08	0.4 ± 0.1	0.48 ± 0.15	31.9 ± 0.4	–18.48 ± 0.4	29.1 ± 0.7	–18.3 ± 0.4	–17.8 ± 0.4
SN2000bh	1.16 ± 0.1	1635.2 ± 0.28	0.02	16.85 ± 0.04	–	–	–	–	–	34.6 ± 0.3	–17.75 ± 0.3	–	–	–
SN2000bk	1.63 ± 0.1	1647.9 ± 0.2	0.17	17.45 ± 0.05	–	–	–	–	–	35.7 ± 0.2	–17.15 ± 0.2	–	–	–
SN2001ba	0.97 ± 0.05	2034.5 ± 0.7	0.03	17.44 ± 0.05	2055.5 ± 0.5	17.25 ± 0.07	15.52 ± 0.09	0.4 ± 0.1	–	35.4 ± 0.2	–18.34 ± 0.2	21.0 ± 0.9	–18.1 ± 0.2	–19.9 ± 0.2
SN2001bt	1.18 ± 0.02	2063.4 ± 0.22	0.12	16.65 ± 0.0	2083.5 ± 0.5	15.76 ± 0.1	15.94 ± 0.20	0.40 ± 0.08	1.52 ± 0.08	34.1 ± 0.4	–18.62 ± 0.4	–	–	–18.2 ± 0.4
SN2001cn	1.15 ± 0.02	2071.6 ± 0.15	0.08	15.83 ± 0.1	–	–	–	–	–	34.1 ± 0.2	–18.52 ± 0.2	–	–	–
SN2001cz	1.05 ± 0.03	2103.9 ± 0.12	0.08	15.65 ± 0.2	2131.5 ± 0.5	15.64 ± 0.2	16.06 ± 0.20	0.4 ± 0.1	–	33.5 ± 0.1	–18.15 ± 0.1	27.6 ± 0.5	–17.9 ± 0.2	–17.3 ± 0.2
SN2001el	1.13 ± 0.04	2182.5 ± 0.5	0.08	12.97 ± 0.04	2204.8 ± 0.5	12.87 ± 0.09	13.14 ± 0.05	0.2 ± 0.1	1.0 ± 0.1	31.3 ± 0.4	–18.47 ± 0.4	22.3 ± 0.7	–18.4 ± 0.4	–18.2 ± 0.8
SN2002bo	1.12 ± 0.03	2356.5 ± 0.2	0.15	13.89 ± 0.03	2381.6 ± 0.5	13.93 ± 0.04	14.48 ± 0.07	0.4 ± 0.1	0.40 ± 0.08	31.8 ± 0.8	–17.91 ± 0.8	25.1 ± 0.5	–17.9 ± 0.8	14.48 ± 0.07
SN2002dj	1.08 ± 0.06	2450.0 ± 0.7	0.12	14.75 ± 0.03	2473.0 ± 0.5	14.65 ± 0.05	–	0.5 ± 0.1	0.5 ± 0.1	32.9 ± 0.2	–18.38 ± 0.2	23.0 ± 0.9	–18.2 ± 0.2	–
SN2003gs	1.83 ± 0.05	3848.5 ± 0.5	0.02	–	–	–	13.48 ± 0.01	0.4 ± 0.1	2.3 ± 0.1	31.7 ± 0.3	–18.42 ± 0.3	–	–	–18.2 ± 0.3
SN2003hv	1.61 ± 0.02	2891.2 ± 0.3	0.01	13.11 ± 0.02	2910.3 ± 0.5	13.19 ± 0.02	13.53 ± 0.03	0.75 ± 0.04	1.9 ± 0.05	31.4 ± 0.3	–18.36 ± 0.3	19.1 ± 0.6	–18.2 ± 0.3	–17.9 ± 0.3
SN2004dt	1.20 ± 0.05	3240.5 ± 0.5	0.08	15.43 ± 0.07	–	–	–	0.03 ± 0.1	–	34.3 ± 0.15	–18.87 ± 0.2	–	–	–
SN2004eo	1.37 ± 0.03	3279.5 ± 0.5	0.06	15.90 ± 0.01	–	–	–	–	–	34.2 ± 0.15	–18.64 ± 0.1	–	–	–
SN2004ey	0.98 ± 0.02	3301.5 ± 0.5	0.05	15.87 ± 0.08	329.1 ± 1	15.59 ± 0.1	15.74 ± 0.02	0.08 ± 0.10	0.4 ± 0.1	34.1 ± 0.1	–18.52 ± 0.2	27.6 ± 1.1	–18.5 ± 0.1	–18.4 ± 0.1
SN2004gs	1.54 ± 0.01	3357.5 ± 0.5	0.05	17.53 ± 0.05	–	–	–	–	–	35.3 ± 0.1	–17.77 ± 0.15	–	–	–
SN2004gu	0.80 ± 0.04	3360.0 ± 0.5	0.10	–	–	–	–	–	–	36.4 ± 0.1	–	–	–	–

Table 15. continued.

SN	$\Delta m_{15}(B)$	$T(B_{\max})$	A_X	m_1	$T(X_2)$	m_2	m_0	$\Delta m_{15}(X)$	$\Delta m_{40}(X)$	μ	$M_{1,X}$	$t_{2,X}$	$M_{2,X}$	$M_{0,X}$
(1)	(2)	(3)	(4)	(5)	(6)	(7)	(8)	(9)	(10)	(11)	(12)	(13)	(14)	(15)
SN2005A	1.17 ± 0.03	3380.0 ± 0.5	0.43	–	–	–	––	–	–	34.4 ± 0.06	–	–	–	–
SN2005M	0.85 ± 0.01	3406.0 ± 0.5	0.03	16.55 ± 0.05	–	–	16.53 ± 0.04	0.13 ± 0.08	–	35.1 ± 0.1	-18.7 ± 0.1	–	–	-18.6 ± 0.1
SN2005am	1.48 ± 0.02	3436.1 ± 0.5	0.02	14.46 ± 0.05	–	–	–	–	–	33.6 ± 0.2	–	–	–	–
SN2005al	1.22 ± 0.04	3430.0 ± 0.5	–0.0	16.00 ± 0.05	3451.0 ± 0.1	15.85 ± 0.05	16.03 ± 0.05	–	–	34.1 ± 0.1	-18.4 ± 0.1	21.0 ± 0.5	-18.2 ± 0.1	-18.1 ± 0.1
SN2005ag	0.86 ± 0.01	3416.8 ± 1.0	0.03	19.44 ± 0.05	–	–	–	–	–	37.5 ± 0.1	–	–	–	–
SN2005el	1.29 ± 0.01	$3645. \pm 0.5$	0.01	15.87 ± 0.05	–	–	–	–	–	33.9 ± 0.15	–	–	–	–
SN2005eq	0.72 ± 0.02	3655.5 ± 0.5	0.07	17.26 ± 0.05	–	–	–	–	–	35.3 ± 0.15	–	–	–	–
SN2005hc	0.90 ± 0.01	3668.7 ± 0.5	0.03	18.06 ± 0.14	–	–	–	–	–	36.5 ± 0.05	–	–	–	–
SN2005iq	1.24 ± 0.01	3687.5 ± 0.5	0.00	17.90 ± 0.10	–	–	–	–	–	32.9 ± 0.15	–	–	–	–
SN2005kc	1.14 ± 0.01	3698.6 ± 0.5	0.11	15.82 ± 0.05	–	–	–	–	–	33.9 ± 0.05	–	–	–	–
SN2005ke	1.76 ± 0.01	3700.7 ± 0.5	0.02	–	–	–	–	–	–	31.4 ± 0.15		–		–
SN2005ki	1.27 ± 0.02	3706.8 ± 0.5	0.00	16.54 ± 0.05	–	–	–	–	–	34.6 ± 0.04	–	–	–	–
SN2006D	1.42 ± 0.01	3758.8 ± 0.5	0.04	14.89 ± 0.02	–	–	–	–	–	32.9 ± 0.15	-18.36 ± 0.2	–	–	–
SN2006X	1.09 ± 0.01	3786.8 ± 0.5	0.52	–	–	–	–	–	–	31.0 ± 0.07	–	–	–	–
SN2006ax	0.99 ± 0.02	3828.5 ± 0.5	0.00	16.04 ± 0.02	–	–	–	–	–	34.3 ± 0.05	–	–	–	–
SN2006bh	1.41 ± 0.01	3833.9 ± 0.5	0.00	15.27 ± 0.05	–	–	–	–	–	33.3 ± 0.1	–	–	–	–
SN2006eq	1.66 ± 0.06	3976.0 ± 0.5	0.08	19.03 ± 0.05	–	–	–	–	–	36.5 ± 0.1	–	–	–	–
SN2006gt	1.66 ± 0.06	4002.7 ± 0.5	0.07	18.82 ± 0.05	–	–	–	–	–	36.5 ± 0.1	–	–	–	–
SN2008fv	0.96 ± 0.05	3749.8 ± 0.2	0.07	14.99 ± 0.06	3780.1 ± 0.5	15.00 ± 0.05	15.39 ± 0.02	0.49 ± 0.09	0.53 ± 0.09	33.2 ± 0.2	-18.2 ± 0.8	30.3 ± 0.5	-18.1 ± 0.8	-17.81 ± 0.2

Notes. (1): SN name; (2) Decline rate in the B-band; (3): Epoch of the B-band maximum −2 450 000 days; (4): total extinction derived by assuming the standard absorption coefficient $R_V = 3.1$ for the Galactic dust and $R_V = 3.2$ for the host galaxies dust, as found by Folatelli et al. (2010); (5): apparent magnitude at maximum in the X-bands, as labeled at the end of Table; (6): epoch of secondary maximum in the X-bands; (7): apparent magnitude at secondary maximum in the X-bands; (8): apparent magnitude at local minimum in the X-bands; (9): decline rate in the X-band measured as the difference in magnitudes between 15 days since the X-band maximum and the peak magnitude; (10): decline rate in the X-band measured as the difference in magnitudes between 40 days since the X-band maximum and the peak magnitude; (11): distance modulus as derived by different methods; (12): absolute magnitude at maximum in the X-band; (13): epoch of secondary maximum since the B-band maximum; (14): absolute magnitude at secondary maximum in the X-bands; (15): absolute magnitude at local minimum in the X-bands. All the magnitudes listed in this table are not corrected for Galactic and host galaxy reddening.

References. [1] Frogel et al. (1987); [2] Phillips et al. (2006); [3] Krisciunas et al. (2004b); [4] Krisciunas et al. (2004c); [5] Valentini et al. (2003); [6] Krisciunas et al. (2001); [7] Krisciunas et al. (2003); [8] Pignata et al. (2008); [9] Krisciunas et al. (2009); [10] Leloudas et al. (2009); [11] Biscardi et al. (in prep.); [12] Folatelli et al. (2010); [13] this work; [a] Ajhar et al. (2001); [b] Willick et al. (1997); [c] Tully (1988); [d] Terry et al. (2002); [e] Tonry et al. (2001); [f] Saha et al. (2006). [*] μ kinematic, as derived assuming the recession velocity from the NED database; For Tonry et al. and Ajhar et al. μs, we apply the correction of −0.16 mag as prescribed by Jensen et al. (2003).